AD-A062 885 TEMPLE UNIV PHILADELPHIA PA DEPT OF CHEMISTRY F/G 11/9
MECHANISM OF PYROELECTRICITY IN POLYVINYLIDENE FLUORIDE FILMS.(U)
NOV 78 K TAKAHASHI, R E SALOMON, M M LABES DAAG29-76-G-0040
UNCLASSIFIED ARO-13268.1-C NL

1 OF 1
ADA
062885

END
DATE
FILMED
3 -79
DDC

Unclassified

SECURITY CLASSIFICATION OF THIS PAGE (When Data Entered)

(12)

(19) **REPORT DOCUMENTATION PAGE**

READ INSTRUCTIONS BEFORE COMPLETING FORM

1. REPORT NUMBER: 13268.1-C (18) ARO
2. GOVT ACCESSION NO.
3. RECIPIENT'S CATALOG NUMBER

4. (6) TITLE (and Subtitle): Mechanism of Pyroelectricity in Polyvinylidene Fluoride Films.
5. (9) TYPE OF REPORT & PERIOD COVERED: Final Report 1 Oct 75 - 31 Oct 78
6. PERFORMING ORG. REPORT NUMBER

7. (10) AUTHOR(s): K. Takahashi, R. E. Salomon, M. M. Labes
8. (15) CONTRACT OR GRANT NUMBER(s): DAAG29-76-G-0040

9. PERFORMING ORGANIZATION NAME AND ADDRESS: Temple University, Philadelphia, Pennsylvania 19122
10. PROGRAM ELEMENT, PROJECT, TASK AREA & WORK UNIT NUMBERS

11. CONTROLLING OFFICE NAME AND ADDRESS: U. S. Army Research Office, P. O. Box 12211, Research Triangle Park, NC 27709
12. (11) REPORT DATE: November 1978
13. NUMBER OF PAGES: 66

14. MONITORING AGENCY NAME & ADDRESS (if different from Controlling Office)
15. SECURITY CLASS. (of this report): Unclassified
15a. DECLASSIFICATION/DOWNGRADING SCHEDULE

LEVEL II

16. DISTRIBUTION STATEMENT (of this Report)

(12) 68p.

Approved for public release; distribution unlimited.

DDC RECEIVED JAN 4 1979 F

17. DISTRIBUTION STATEMENT (of the abstract entered in Block 20, if different from Report)

18. SUPPLEMENTARY NOTES

The view, opinions, and/or findings contained in this report are those of the author(s) and should not be construed as an official Department of the Army position, policy, or decision, unless so designated by other documentation.

19. KEY WORDS (Continue on reverse side if necessary and identify by block number)

Pyroelectricity
Polyvinylidene Fluoride Films
Polymers
Polar Polymers
Pyroelectric Coefficients
Polymeric Pyroelectrics

20. ABSTRACT (Continue on reverse side if necessary and identify by block number)

The objectives of this study were the exploration of the mechanism(s) of pyroelectricity in polymers in order to achieve the highest possible pyroelectric coefficients with polar polymers, a determination of whether or not polyvinylidene fluoride (PVF_2) is an optimum material in this regard, and a determination of means of improving the performances of these polymeric pyroelectrics. This report contains the results of this study.

DD FORM 1 JAN 73 1473 EDITION OF 1 NOV 65 IS OBSOLETE

Unclassified 407 646 LB

SECURITY CLASSIFICATION OF THIS PAGE (When Data Entered)

AD A062885

DDC FILE COPY

MECHANISM OF PYROELECTRICITY IN POLYVINYLIDENE FLUORIDE FILMS

Department of Chemistry

Temple University

Philadelphia, PA 19122

FINAL REPORT

November 1978

Grant No. DAAG29-76-G-0040

U. S. Army Research Office

Department of the Army

Research Triangle Park, NC 27709

FINAL REPORT

1. ARO PROPOSAL NUMBER: 13268C

2. PERIOD COVERED BY REPORT: October 1, 1975 through October 31, 1978

3. TITLE OF PROPOSAL: Mechanism of Pyroelectricity in Polyvinylidene Fluoride Films

4. CONTRACT OR GRANT NUMBER: DAAG29-76-G-0040

5. NAME OF INSTITUTION: Temple University

6. AUTHOR(S) OF REPORT: K. Takahashi, R. E. Salomon and M. M. Labes

7. LIST OF MANUSCRIPTS SUBMITTED OR PUBLISHED UNDER ARO SPONSORSHIP DURING THIS PERIOD, INCLUDING JOURNAL REFERENCES:

   See Attached

8. SCIENTIFIC PERSONNEL SUPPORTED BY THIS PROJECT AND DEGREES AWARDED DURING THIS REPORTING PERIOD:

   K. Takahashi -- Post Doctoral Research Associate

   C. S. Bak-- Post Doctoral Research Associate

   H. Lee -- Graduate Research Assistant (Ph.D, January 1978)

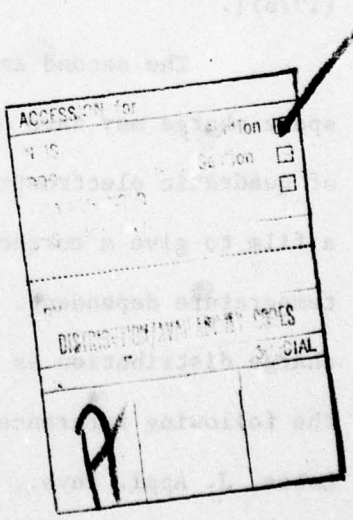

BRIEF OUTLINE OF RESEARCH FINDINGS

The objectives of this study were the exploration of the mechanism(s) of pyroelectricity in polymers in order to achieve the highest possible pyroelectric coefficients with polar polymers, a determination of whether or not polyvinylidene fluoride (PVF_2) is an optimum material in this regard, and a determination of means of improving the performances of these polymeric pyroelectrics.

Theoretical Work

Theoretical work was done on developing three models for pyroelectricity in polymers. The first of these deals with the rotation of rigid cylindrical dipolar rods in a viscous fluid. The importance of this model stems from the difficulties inherent in either the rotation of portions of a polar chain segment or the rotation of an entire chain in the presence of a crystalline environment created by other polymer chains. See paper (1) listed below. This particular approach has received some support from the findings of Kepler et al [R. G. Kepler and R. A. Anderson, J. Appl. Phys. 49, 4918 (1978)].

The second and third models deal with the possible effects that space charge may have on pyroelectric activity. We consider the phenomena of quadratic electrostriction and how it may interact with a space charge in a film to give a current when the quadratic electrostriction constant is temperature dependent. Although the film itself is homogeneous, the space charge distribution is not. Evidence for this inhomogeniety can be found in the following references: [L. F. Hu, K. Takahashi, R. E. Salomon and M. M. Labes, J. Appl. Phys., to appear Feb. 1979 (see paper (8) listed below)] and

[R. L. Peterson, G. W. Day, P. M. Gruzensky and R. J. Phelan, J. Appl. Phys. 45, 3296 (1974]. Lastly, we consider the case of an inhomogeneous film in which the dielectric constants and thermal expansion coefficients vary with position. See papers (2) and (3) listed below.

Pyroelectricity in PVF_2-PMMA Blends

Polymer blends of PVF_2 with both poly(methyl methacrylate) and poly(vinyl fluoride) were prepared and evaluated for pyroelectric activity. Percent crystallinity and extent of α, β, γ and amorphous phases were evaluated by both x-ray diffraction and infrared spectroscopy. The correlations observed are supportive of a dipole reorientation model for pyroelectricity. See paper (4) listed below.

Electrode Effects on the Poling of PVF_2

By analysis of steady-state current-time-voltage-temperature relationships, it was concluded that a Richardson-Schottky process is dominant at the high fields and temperatures typically employed in poling PVF_2. Data on pyroelectric behavior with different layer configurations and with different electrode configurations suggest that hole injection is of major importance. See paper (5) listed below.

Mechanistic Studies of Pyroelectricity in Polymers

Inferences as to the mechanisms of pyroelectricity in PVF_2 were made from the experimental results obtained with different layer configurations, different electrode configurations, polymer blends of PVF_2 with poly(methyl methacrylate) and poly(vinyl fluoride), and a copolymer of 20% acrylonitrile-80% vinylidene chloride (P(AN-VCl_2)). The importance of the dipole-reorientation process and hole injection during poling were both

emphasized in the interpretation of these experiments. See paper (6) listed below.

High Voltage Poling at Low Temperature

In "Fluorinert" and vacuum media, the thermal breakdown voltage of PVF_2 films has been greatly enhanced. The poling temperature was extended down to $-78^{o}C$ using this dielectric liquid. The results show that even at a poling temperature of $-72^{o}C$, a large pyroelectric coefficient of 2.12 $nC \cdot cm^{-2}\ {}^{o}K^{-1}$ was obtained at a poling field of 4×10^{6} $V \cdot cm^{-1}$. See paper (7) listed below.

Frequency Dependence of Pyroelectric Current in PVF_2

The frequency and temperature dependences of pyroelectric activity in PVF_2 have been studied from $10^{o}K$ to $369^{o}K$ using both mechanically chopped and steady state radiation as the heat source. From these data, thermal diffusivity and a parameter indicating the polarization inhomogeneity were calculated using a Fourier transform technique. The pyroelectric coefficients were moderately temperature dependent from $10^{o}K$ to the glass transition temperature and exhibited a T^2 dependence from the glass transition temperature to $369^{o}K$. See paper (8) listed below.

Pyroelectric Effect in Chiral Smectic C and H Liquid Crystals (partial support)

The ferroelectric-like structure of the chiral smectic C and H phases was confirmed by the experimental observation of a pyroelectric effect. See paper (9) listed below.

Pyroelectric Effect in $P(AN\text{-}VCl_2)$

$P(AN\text{-}VCl_2)$ showed a small, negative pyroelectric current. A space-charge model was invoked to help explain the negative pyroelectricity observed

in this material (which is known to trap charge very effectively). See paper (10) listed below.

Discharge Currents in PVF_2

To evaluate the nature of the processes in which trapped charge is released, the change of discharge currents for a sample after charging at various dc voltages was measured. The discharge characteristics after the application of high voltages were markedly different from those obtained with low voltages. This observation indicates that the trap states which are filled at high voltages have a trap level distribution and detrapping rate which are significantly different from the traps associated with low voltages. Since this high voltage range corresponds to the onset of efficient poling, the trap states filled during poling may play an important role in pyroelectricity.

LIST OF MANUSCRIPTS SUBMITTED OR PUBLISHED UNDER ARO SPONSORSHIP DURING THIS PERIOD, INCLUDING JOURNAL REFERENCES.

(1) B. K. Oh, M. M. Labes and R. E. Salomon, J. Chem. Phys. 64, 3375 (1976).

(2) R. E. Salomon, H. Lee, C. S. Bak and M. M. Labes, J. Appl. Phys. 47, 4206 (1976).

(3) R. E. Salomon, B. K. Oh and M. M. Labes, J. Appl. Phys. 47, 1710 (1976).

(4) H. Lee, R. E. Salomon and M. M. Labes, Macromolecules 11, 171 (1978).

(5) K. Takahashi, H. Lee, R. E. Salomon and M. M. Labes, J. Appl. Phys. 48, 4694 (1977).

(6) K. Takahashi, H. Lee, R. E. Salomon and M. M. Labes, Organic Coatings and Plastics Chemistry 38, 328 (1978).

(7) K. Takahashi, R. E. Salomon and M. M. Labes, Bull. Amer. Phys. Soc. 23, 377 (1978).

(8) L. F. Hu, K. Takahashi, R. E. Salomon and M. M. Labes, J. Appl. Phys. (to appear Feb. 1979).

(9) L. J. Yu, H. Lee, C. S. Bak and M. M. Labes, Phys. Rev. Lett. 36, 388 (1976), partial support.

(10) H. Lee, R. E. Salomon and M. M. Labes, J. Appl. Phys. (submitted).

Relaxation of polar cylinders in strong electric fields*

Byung K. Oh, M. M. Labes, and R. E. Salomon

Department of Chemistry, Temple University, Philadelphia, Pennsylvania 19104
(Received 29 October 1975)

The problem of rotational diffusion of a polar cylinder about its long axis in an electric field has been solved. The solutions apply to the high as well as the low field limits. The results are presented as a function of a reduced time and the variable κ, which is a measure of the ratio of mean electrical energy to thermal energy. Asymptotic expansions are obtained for the distribution function and the fractional polarization. The eigenvalues and even solution of a Whittaker–Hill–Ince differential equation have been calculated as functions of κ. Asymptotic expansions of the eigenvalue and solution of this equation are given.

I. INTRODUCTION

The general theoretical problem of rotational diffusion in the presence of external fields has a number of applications. Recently we studied a problem of this type, namely, rotation of polar cylinders immersed in a viscous fluid in an external electric field with the moment normal to the cylinder axis. This two-dimensional problem was analyzed in a manner which provides numerical solutions for various values of the diffusion constant and electric field. By way of comparison, we note that the problem of relaxation of spherical dipoles which were partially aligned in an electric field was treated by Debye[1] in his classic work on dielectric relaxation. Since dielectric relaxation is typically studied at fields sufficiently low so as to avoid saturation, various approximations (expansions) are made which simplify the mathematics considerably. Such approximations are part of the Debye theory.

Our interest in this problem stemmed from a search for a model which might explain the phenomena of pyroelectricity produced in polyvinylidene fluoride (PVF_2) which has been poled (maintained at a very high field at an elevated temperature).[2] The limited structural data suggested to us that the phenomena might be due to the rotation of rigid rods of crystalline PVF_2 (consisting of the polar planar zig–zag phase) in an apolar, amorphous matrix.[3] The kinetics of both poling and depoling as well as the equilibrium spontaneous polarization were the objects of our attention.

A search of the literature failed to reveal a general solution of this problem which could be applied to the situation of high fields, i.e., $E\mu/kT \gg 1$, where E is the field, μ is the moment, T is the absolute temperature, and k is the Boltzmann constant. Lauritzen and Zwanzig studied a two-site model for the relaxation of a single axis rotor in which the relaxation occurs in the presence of a potential energy barrier.[4] Although our study was motivated by a desire to explain the pyroelectric data obtained with PVF_2, it is clear that the results are applicable to other problems such as electrical polarization and relaxation in strong fields.

II. FORMULATION OF THE PROBLEM

In general, the distribution function f for a diffusion process occurring in the presence of an external field is governed by the equation[5]

$$\frac{\partial f}{\partial t} = D_g \nabla^2 f + \mathrm{div}(\alpha f \nabla V) , \tag{1}$$

where D_g is the general diffusion coefficient, α is the orientational mobility, V is the potential energy, and ∇ and ∇^2 bear their usual meanings. We apply Eq. (1) to the case of the polar rods in a nonpolar viscous medium. We assume that the only motion allowed for the rod is reorientation about the long axis. We further assume no deformation in the dimensions of the rod. Introducing cylindrical coordinates we obtain from Eq. (1)

$$\frac{\partial f}{\partial t} = D\left(\frac{\partial^2 f}{\partial \theta^2} + \frac{\alpha v_c P_0 E}{DR^2}\frac{\partial}{\partial \theta} f \sin\theta\right) , \tag{2}$$

where D is the rotational diffusion coefficient, R is the radius of the rod, v_c is the volume of the rod, P_0 is the saturation polarization per unit volume of the rod, E is the field acting on the dipole, and θ is the angle between the field and the polarization vector of the rod. At equilibrium, $\partial f/\partial t = 0$, and f should be proportional to the Boltzmann factor $\exp(v_c P_0 E \cos\theta/kT)$ from which we obtain

$$\alpha = DR^2/kT . \tag{3}$$

III. DEPOLARIZATION

We first consider the decay of the polarization of already oriented rods. In the absence of the external field, Eq. (2) becomes

$$\frac{\partial f}{\partial t} = D\frac{\partial^2 f}{\partial \theta^2} . \tag{4}$$

The distribution function f is even and periodic:

$$f(\theta, t) = f(-\theta, t) = f(\theta \pm 2\pi n, t), \quad n = 0, 1, 2, \ldots \tag{5}$$

The initial condition is given by

$$f(\theta, 0) = \exp(\kappa \cos\theta)/2\pi I_0(\kappa) , \tag{6}$$

where $I_0(\kappa)$ is a modified Bessel function[6] and

$$\kappa = v_c P_0 E/kT . \tag{7}$$

We solve Eq. (4) by separation of variables. Substitution of

$$f(\theta, t) = X(\theta) Y(t) \tag{8}$$

into Eq. (4) yields

$$X_\lambda(\theta) = A_\lambda \cos\lambda\theta + B_\lambda \sin\lambda\theta , \tag{9}$$

$$Y_\lambda(t) = e^{-D\lambda^2 t} . \tag{10}$$

Owing to the periodic boundary condition given by Eq. (5), we have

$$\lambda = \pm m, \quad m = 0, 1, 2, \ldots , \tag{11}$$

which leads Eq. (8) to the form

$$f(\theta, t) = A_0 + \sum_{m=1}^{\infty} e^{-Dm^2 t}(A_m \cos m\theta + B_m \sin m\theta) . \tag{12}$$

After determining the coefficients by incorporating Eq. (6) with Eq. (12), we obtain for the distribution function $f(\theta, t)$

$$f(\theta, t) = \frac{1}{2\pi} + \frac{1}{\pi I_0(\kappa)} \sum_{m=1}^{\infty} e^{-Dm^2 t} I_m(\kappa) \cos m\theta . \tag{13}$$

The residual polarization corresponding to this distribution function is given by

$$\overline{\cos\theta} = \int_0^{2\pi} f \cos\theta \, d\theta = [I_1(\kappa)/I_0(\kappa)] e^{-Dt} , \tag{14}$$

which shows that decay of polarization from the equilibrium state is a first order rate process.

IV. POLARIZATION

Let us now consider the solution of Eq. (2) which deals with the polarization of initially unpoled sample. As before, we solve the differential equation by separation of variables; substitution of Eq. (8) into Eq. (2) yields

$$Y_\lambda = e^{-D\lambda^2 t} , \tag{15}$$

$$\frac{d^2 X}{d\theta^2} + \kappa \sin\theta \frac{dX}{d\theta} + (\lambda^2 + \kappa \cos\theta) X = 0 . \tag{16}$$

If we let $\theta = 2x$, Eq. (16) becomes a Whittaker–Hill–Ince differential equation[7–9] (i.e., $p = -2$, $\xi = 2\kappa$, and $\eta = 4\lambda^2$ in the standard notations). However, the solution corresponding to the present problem, i.e., $p = -2$, is not available in the literature.

Following Ince,[8] we denote the even and odd solutions by $C_{-2}(\theta, \kappa)$ and $S_{-2}(\theta, \kappa)$, respectively;

$$C_{-2}(\theta, \kappa) = \sum_{n=0}^{\infty} a_n(\kappa) \cos n\theta , \tag{17}$$

$$S_{-2}(\theta, \kappa) = \sum_{n=0}^{\infty} b_n(\kappa) \sin n\theta . \tag{18}$$

Since by assumption $f(\theta, t)$ should be even and have the periodicity of 2π, we need only the even solution. Substituting Eq. (17) into Eq. (16) and gathering terms having the same value of $\cos(n\theta)$, we obtain the following recurrence relation between the coefficients a_n;

$$\begin{aligned} &\lambda^2 a_0 = 0 , \\ &3a_0 + (\lambda^2 - 1)(2/\kappa) a_1 - a_2 = 0 , \\ &n a_{n-1} + (\lambda^2 - n^2)(2/\kappa) a_n - n a_{n+1} = 0 , \quad n \geq 2 . \end{aligned} \tag{19}$$

Notice that $a_0 = 0$, if $\lambda \neq 0$. Eigenvalues λ which satisfy the above recurrence relation give periodic solutions. It is customary to arrange λ according to the limiting behaviors at $\kappa \to 0$. That is, from Eq. (16) we can show that

$$\lim_{\kappa \to 0} \lambda_m^2 \to m^2, \quad m = 0, 1, 2, \ldots \tag{20}$$

The corresponding solution will be denoted by the superscript m, i.e., C_{-2}^m. It is noted that the smallest eigenvalue $\lambda = 0$ leads to the equilibrium solution given by Eq. (6), as will be shown later.

Using Eq. (20), we write the distribution function as follows:

$$f(\theta, t) = f(\theta, \infty) + \sum_{m \geq 1} e^{-D\lambda_m^2 t} A_m C_{-2}^m . \tag{21}$$

We determine the equilibrium solution $f(\theta, \infty)$ and the coefficient A_m using the initial condition assumed to be a random distribution of dipolar axes;

$$f(\theta, 0) = \frac{1}{2\pi}, \quad \int_0^{2\pi} f(\theta, 0) \, d\theta = 1 . \tag{22}$$

The equilibrium solution satisfies the following differential equation:

$$\frac{d^2 f(\theta, \infty)}{d\theta^2} + \kappa \frac{d}{d\theta} f(\theta, \infty) \sin\theta = 0 , \tag{23}$$

obtained by letting $\lambda = 0$ in Eq. (16). Its even solution which we are interested in is nothing but Eq. (6). To determine the coefficient A_m we use Ince's normalization condition for C_{-2}^m given by

$$\sum_{n \geq 1} |a_n^m|^2 = 1, \quad m \geq 1 \tag{24}$$

and the following orthogonality,

$$\begin{aligned} &\frac{1}{\pi} \int_0^{2\pi} e^{-\kappa \cos\theta} C_{-2}^m C_{-2}^l \, d\theta \\ &= \delta_{m,l} \sum_{n, n' \geq 1} (-1)^{n+n'} a_n^m a_{n'}^l (I_{n+n'} + I_{n-n'}) , \end{aligned} \tag{25}$$

where $\delta_{m,l}$ is the Kronecker delta. This orthogonality can be proven using Eq. (16) and the periodicity of C_{-2}^m. Letting $t = 0$ in Eq. (21) and applying Eqs. (24) and (25) to it, we obtain the following result for A_m:

$$A_m = Z_m / \pi I_0 ; \tag{26}$$

$$Z_m = \sum_{n \geq 1} (-1)^n a_n^m I_0 I_n \left(\sum_{n, n' \geq 1} (-1)^{n+n'} a_n^m a_{n'}^m (I_{n+n'} + I_{n-n'}) \right)^{-1} .$$

Thus, the distribution function given by Eq. (21) takes the form

$$f(\theta, t) = \frac{1}{2\pi I_0} \left(e^{\kappa \cos\theta} + 2 \sum_{m \geq 1} e^{-D\lambda_m^2 t} Z_m C_{-2}^m \right) . \tag{27}$$

Before going further it is interesting to observe from Eqs. (22) and (27) that

$$I_n = -\sum_{m \geq 1} a_n^m Z_m . \tag{28}$$

When κ is small, Eq. (27) becomes

$$f(\theta, t) = \frac{1}{2\pi} [1 + \kappa(1 - e^{-Dt}) \cos\theta] + O(\kappa^2) , \tag{29}$$

where use has been made of the asymptotes of C_{-2}^m and λ_m^2 given by

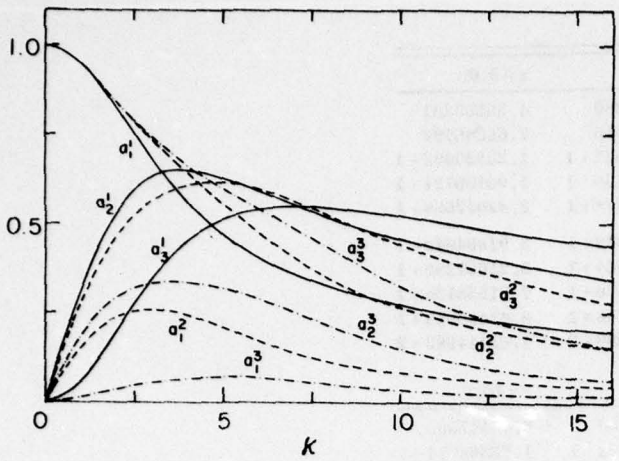

FIG. 1. Coefficients $a_n^m(\kappa)$ of the Ince polynomial $C_{-2}^m(\kappa, \theta)$ vs κ for several values of m and n.

$$C_{-2}^m = \cos m\theta + \frac{\kappa}{2}\left(\frac{m+1}{2m+1}\cos(m+1)\theta + \frac{m-1}{2m-1}\cos(m-1)\theta\right) + \frac{\kappa^2}{16}\left(\frac{m+2}{2m+1}\cos(m+2) + \frac{m-2}{2m-1}\cos(m-2)\theta\right) + \cdots , \tag{30}$$

$$\lambda_m^2 = m^2 + \frac{m^2}{8m^2-2}\kappa^2 + \cdots . \tag{31}$$

The derivation is shown in Appendix A. When κ is not too small, we need to know the eigenvalues and coefficients as functions of κ and m. As pointed out previously, the case $m=0$ gives the equilibrium solution given by Eq. (6). When $m \geq 1$, the recurrence formula given by Eq. (19) becomes

$$(\lambda^2 - 1)(2/\kappa)a_1 - a_2 = 0 ,$$
$$a_{n-1} + [(\lambda^2 - n^2)/n](2/\kappa)a_n - a_{n+1} = 0, \quad n \geq 2 . \tag{32}$$

Since this is a three-term recurrence formula, we may solve it numerically using the continued fraction method developed for Mathieu's function.[10] The detailed procedure has been described in Appendix B. We have summarized the results in Table I and Fig. 1, which show the eigenvalues and the first few a_n^m, respectively. Notice from Table I that for $\kappa < 10$ the asymptotic expression given by Eq. (31) becomes quite good. We also note from Fig. 1 that $a_n^m \to \delta_{m,n}$ as $\kappa \to 0$.

Finally, the fractional polarization corresponding to the distribution function given by Eq. (27) takes the form

$$\overline{\cos\theta} = (I_1/I_0)\left(1 + \sum_{m\geq 1} e^{-D\lambda_m^2 t}(a_1^m/I_1)Z_m\right) . \tag{33}$$

In Table II we have presented values of the coefficients $(a_1^m/I_1)Z_m$. In Fig. 2 we have plotted $\overline{\cos\theta}$ as a function of the reduced time, Dt, for several values of κ. Since the scaling factor of the abscissa is D, the average polarization depends strongly on D and increases as D decreases.

When κ is small, Eq. (29) yields the following expression for $\overline{\cos\theta}$,

$$\overline{\cos\theta} = \tfrac{1}{2}\kappa(1 - e^{-Dt}) + O(\kappa^2) , \tag{34}$$

which is comparable to the well-known Debye solution[1] for Eq. (2) in the three-dimensional case. When $\kappa \to \infty$, Eq. (33) reduces to the form

$$\overline{\cos\theta} \sim 1 + \frac{1}{2}\sum_{m\geq 1} e^{-D\lambda_m^2 t} a_1^m \left(\sum_{n\geq 1}(-)^n a_n^m\right)^{-1} , \tag{35}$$

for which we have used the fact that $I_n(\kappa)$ depends only on κ as $\kappa \to \infty$.

One of the obvious applications of the present work is in the calculation of the frequency dependence of nonlinear dielectrics which conform to this model. Another application is the calculation of the time needed to achieve a specific polarization in pyroelectric polymers. Unfortunately, to make such a calculation one must have a knowledge of the temperature dependence of the rotational diffusion coefficient as well as the rod (crystallite) dimensions, both of which are not available at this moment.

APPENDIX A: ASYMPTOTIC EXPANSIONS OF $C_{-2}^m(\theta,\kappa)$ AND $\lambda_m^2(\kappa)$ FOR SMALL κ

For this purpose it is most convenient to introduce another normalization condition that the coefficient a_n^m of C_{-2}^m is taken as unity. We then make the following perturbation expansions of C_{-2}^m and λ_m^2:

$$C_{-2}^m = \cos m\theta + \kappa f_1 + \kappa^2 f_2 + \cdots , \tag{A1}$$

$$\lambda_m^2 = m^2 + \kappa c_1 + \kappa^2 c_2 + \cdots , \tag{A2}$$

where f_i and c_i are the expansion coefficients. Substituting the above two equations into Eq. (16) and gathering terms having the same powers of κ, we arrived at

$$\kappa;\ \frac{d^2 f_1}{d\theta^2} + m^2 f_1 = -\tfrac{1}{2}[(m+1)\cos(m+1)\theta - (m-1)\cos(m-1)\theta + 2c_1\cos m\theta] , \tag{A3}$$

$$\kappa^2;\ \frac{d^2 f_2}{d\theta^2} + m^2 f_2 = -[c_2\cos m\theta + f_1(c_1 + \cos m\theta) + (df_1/d\theta)\sin\theta] . \tag{A4}$$

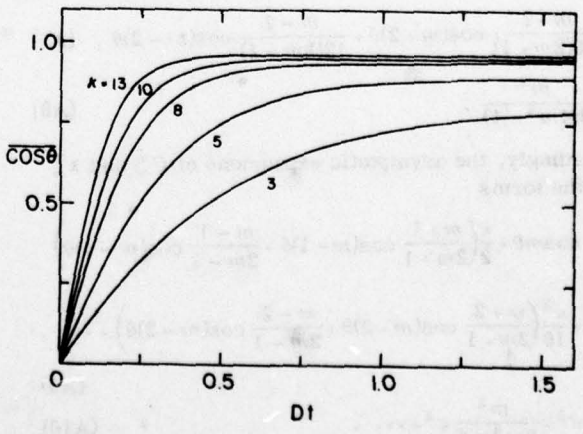

FIG. 2. Fractional polarization $\overline{\cos\theta}$ as functions of a reduced time Dt for several values of κ.

TABLE I. Eigenvalues $\lambda_m^2(\kappa)$ of Eq. (16).

m	$\kappa=1.0$	$\kappa=2.0$	$\kappa=3.0$	$\kappa=4.0$	$\kappa=5.0$
1	1.16549653	1.64736539	2.39819200	3.33421380	4.35503251
2	4.13375275	4.54058837	5.24051706	6.27057315	7.66286492
3	9.12877537	9.51757750	1.01740608+1	1.11118622+1	1.23525093+1
4	1.61271021+1	1.65098299+1	1.71524814+1	1.80623456+1	1.92499121+1
5	2.51263391+1	2.55062757+1	2.61425761+1	2.70398818+1	2.82047668+1
6	3.61259276+1	3.65043525+1	3.71372041+1	3.80277078+1	3.91804042+1
7	4.91256804+1	4.95031953+1	5.01339662+1	5.10203664+1	5.21657280+1
8	6.41255204+1	6.45024452+1	6.51318649+1	7.02219026+1	7.21558434+1
9	8.11254109+1	8.15019314+1	8.21304243+1	8.30123288+1	8.41496619+1
10	1.00125332+2	1.00501564+2	1.01129393+2	1.02009988+2	1.03144983+2
m	$\kappa=6.0$	$\kappa=7.0$	$\kappa=8.0$	$\kappa=9.0$	$\kappa=10.0$
1	5.39012510	6.41609316	7.43276834	8.44375039	9.45147505
2	9.39411012	1.13673096+1	1.34539231+1	1.55565222+1	1.76368774+1
3	1.39287201+1	1.58841422+1	1.82524014+1	2.10098415+1	2.40514539+1
4	2.07295110+1	2.25200645+1	2.46475511+1	2.71480348+1	3.00669391+1
5	2.96458423+1	3.13739441+1	3.34024722+1	3.57480333+1	3.84316948+1
6	4.06011824+1	4.22973365+1	4.42776599+1	4.65525978+1	4.91344973+1
7	5.35743556+1	5.52515473+1	5.72036304+1	5.94380156+1	6.19632801+1
8	6.85569545+1	7.02219026+1	7.21558434+1	7.43643635+1	7.68538708+1
9	8.55450212+1	8.72015896+1	8.91231432+1	9.13140621+1	9.37793475+1
10	1.04536481+2	1.06187058+2	1.08099766+2	1.10278138+2	1.12726199+2
m	$\kappa=11.0$	$\kappa=12.0$	$\kappa=13.0$	$\kappa=14.0$	$\kappa=15.0$
1	1.04572395+1	1.14617334+1	1.24653489+1	1.34683273+1	1.44708267+1
2	1.96935409+1	2.17339618+1	2.37641534+1	2.57877263+1	2.78067673+1
3	2.72302238+1	3.04264732+1	3.37641534+1	3.67062649+1	3.97956681+1
4	3.34391208+1	3.72426965+1	4.13691790+1	4.56574555+1	4.99672513+1
5	4.14813143+1	4.49346275+1	4.88383911+1	5.32295746+1	5.80900287+1
6	5.20380296+1	5.52809378+1	5.88854110+1	6.28804784+1	6.73050476+1
7	6.47892928+1	6.79274048+1	7.13907438+1	7.51946912+1	7.93576957+1
8	7.96316446+1	8.27059083+1	8.60859327+1	8.97821835+1	9.38065379+1
9	9.65246449+1	9.95562774+1	1.02881291+2	1.06507519+2	1.20443664+2
10	1.15448474+2	1.18450009+2	1.21736395+2	1.25313792+2	1.29188976+2

Solution of Eq. (A3) takes the form

$$f_1=\frac{m+1}{2(2m+1)}\cos(m+1)\theta+\frac{m-1}{2(2m-1)}\cos(m-1)\theta\ , \qquad \text{(A5)}$$

$$c_1=0\ . \qquad \text{(A6)}$$

Substituting these into Eq. (A4) and solving the resultant equation, we get

$$f_2=\frac{m+2}{16(2m+1)}\cos(m+2)\theta+\frac{m-2}{12(2m-1)}\cos(m-2)\theta\ , \qquad \text{(A7)}$$

$$c_2=\frac{m^2}{2(4m^2-1)}\ . \qquad \text{(A8)}$$

Accordingly, the asymptotic expansions of C_{-2}^m and λ_m^2 take the forms

$$C_{-2}^m=\cos m\theta+\frac{\kappa}{2}\left(\frac{m+1}{2m+1}\cos(m+1)\theta+\frac{m-1}{2m-1}\cos(m-1)\theta\right)$$
$$+\frac{\kappa^2}{16}\left(\frac{m+2}{2m+1}\cos(m+2)\theta+\frac{m-2}{2m-1}\cos(m-2)\theta\right)+\cdots\ , \qquad \text{(A9)}$$

$$\lambda_m^2=m^2+\frac{m^2}{8m^2-2}\kappa^2+\cdots\ . \qquad \text{(A10)}$$

Conversion of Eq. (A9) to Ince's is simple. Since the coefficients d_n^m of $\cos n\theta$ in the above equation are related to those from Ince's as follows,

$$a_n^m=a_m^m d_n^m, \qquad \sum_{n>1}|d_n^m|^2=|a_m^m|^{-2}\ , \qquad \text{(A11)}$$

the conversion factor a_m^m takes the form according to Eq. (B7)

$$a_m^m=1-\frac{\kappa^2}{8}\left[\left(\frac{m+1}{2m+1}\right)^2+\left(\frac{m-1}{2m-1}\right)^2\right]+O(\kappa^4)\ . \qquad \text{(A12)}$$

It is noted that the eigenvalues given by Eq. (A10) are independent of normalization conditions.

APPENDIX B: CALCULATION OF THE EIGENVALUES AND COEFFICIENTS OF $C_{-2}^m(\theta,\kappa)$

We next consider the numerical evaluation of the eigenvalues λ_m for a given κ. The technique is very similar to that for Mathieu's equation.[10] We rewrite Eq. (32) as

$$u_n=\frac{\kappa/2n}{1-(\lambda^2/n^2)+(\kappa/2n)u_{n+1}}\ , \qquad \text{(B1)}$$

where

$$u_n=a_n/a_{n-1}\ . \qquad \text{(B2)}$$

TABLE II. Coefficients $(a_1^m/I_1)Z_m$ in Eq. (33).

m	$\kappa=1.0$	$\kappa=2.0$	$\kappa=3.0$	$\kappa=4.0$	$\kappa=5.0$
1	−1.01539267+00	−1.07605419+00	−1.20501604+00	−1.39233573+00	−1.57689055+00
2	1.54508123−02	7.72315963−02	2.12561871−01	4.21143613−01	6.57084994−01
3	−5.82401371−05	−1.18547184−03	−7.66349381−03	−2.96223394−02	−8.38629686−02
4	9.91503380−08	8.10107679−06	1.18696410−04	8.27199881−05	3.75916995−03
5	−9.56631225−11	−3.13001576−08	−1.03429258−06	−1.28693695−05	−9.20589529−05
6	5.93035995−14	7.76513587−11	5.77901092−09	1.28060413−07	1.43563253−06
7	−2.55888513−17	−1.34053930−13	−2.24581624−11	−8.85499134−10	−1.55333619−08
8	8.12374728−21	1.70255095−16	6.41934174−14	4.50179728−12	1.23487894−10
9	−1.97651747−24	−1.65705469−19	−1.40597167−16	−1.75335479−14	−7.51846271−13
10	3.80221767−28	1.27512732−22	2.43454479−19	5.39838587−17	3.61800356−15
m	$\kappa=6.0$	$\kappa=7.0$	$\kappa=8.0$	$\kappa=9.0$	$\kappa=10.0$
1	−1.70531750+00	−1.78001621+00	−1.82381129+00	−1.85200954+00	−1.87189643+00
2	8.82363872−01	1.09892643+00	1.29723528+00	1.45013449+00	1.55272066+00
3	−1.89486756−01	−3.53221800−01	−5.53652660−01	−7.59921005−01	−9.61699435−01
4	1.28903456−02	3.60445531−02	8.57430616−02	1.76876033−01	3.17187185−01
5	−4.60183616−04	−1.78714884−03	−5.74298086−03	−1.58862683−02	−3.87795806−02
6	1.03837584−05	5.52957348−05	2.34681150−04	8.35260890−04	2.57979310−03
7	−1.62157472−07	−1.17945638−06	−6.57159739−06	−2.98183210−05	−1.14864129−04
8	1.85864752−09	1.84351943−08	1.34523998−09	7.75491106−07	3.70742643−06
9	−1.63072408−11	−2.20394175−10	−2.10389028−09	−1.53839054−08	−9.10725253−08
10	1.13052653−13	2.08108860−12	2.59731823−11	2.40696999−10	1.76244931−09
m	$\kappa=11.0$	$\kappa=12.0$	$\kappa=13.0$	$\kappa=14.0$	$\kappa=15.0$
1	−1.88684699+00	−1.89857480+00	−1.90805277+00	−1.91588550+00	−1.92247370+00
2	1.62033535+00	1.66765596+00	1.70343064+00	1.73055325+00	1.76107077+00
3	−1.15003841+00	−1.30375961+00	−1.41391392+00	−1.49005696+00	−1.54497113+00
4	4.91544947−01	6.84378644−01	8.73134098−01	1.05155858+00	1.20493475+00
5	−8.47045266−02	−1.66148136−01	−2.90975940−01	−4.51884769−01	−6.29042109−01
6	7.07977945−03	1.75465284−02	3.96895870−02	8.23148599−02	1.56415731−01
7	−3.86832935−04	−1.16341631−03	−3.17416209−03	−7.94427706−03	−1.83827295−02
8	1.52148683−05	5.49714654−05	1.78210190−04	5.25756357−04	1.42240970−03
9	−4.54061914−07	−1.96268446−06	−7.51847609−06	−2.59500108−05	−8.08269003−05
10	1.06587027−08	5.50063270−08	2.48312603−07	9.99157322−07	3.53516260−06

Repeated application of Eq. (B1) yields an infinite continued fraction which is convergent according to the rule given by Perron.[11] We write the Nth convergent of u_n as follows:

$$\frac{\kappa/2}{n-1}u_n=\frac{(\frac{1}{2}\kappa)^2/(n-1)n}{1-(\lambda^2/n^2)+}\ \frac{(\frac{1}{2}\kappa)^2/n(n+1)}{1-[\lambda^2/(n+1)^2]+}$$

$$\cdots\frac{\kappa^2/(N+n-1)(N+n)}{1-[\lambda^2/(N+n)^2]}\equiv E_{N+n}\,. \tag{B3}$$

We can also write Eq. (B1) into the following finite continued fraction,

$$-\frac{(\kappa/2)}{(n-1)}u_n=1-\frac{\lambda^2}{(n-1)^2}-\tfrac{1}{2}\kappa/[(n-2)u_{n-1}]$$

$$=1-\frac{\lambda^2}{(n-1)^2}+F_n; \tag{B4}$$

$$F_n=\frac{(\frac{1}{2}\kappa)^2/(n-1)(n-2)}{1-[\lambda^2/(n-2)^2]+}\ \frac{(\frac{1}{2}\kappa)^2/(n-2)(n-3)}{1-[\lambda^2/(n-3)^2]+}$$

$$\cdots\frac{(\frac{1}{2}\kappa)^2/(3\times2)}{1-(\lambda^2/4)+}\ \frac{(\frac{1}{2}\kappa)^2/2}{1-\lambda^2}\,, \tag{B5}$$

with $F_2=0$.

Then, defining the function G_n as follows

$$G_n=1-\frac{\lambda^2}{(n-1)^2}+F_n+E_{N+n};\quad n\geq 2, \tag{B6}$$

we see that G_n will be zero for $\lambda=\lambda_m$. We now describe the procedure of calculating λ_m. We first specify m. We let $n=m+1$ and choose an appropriate N value. Using an approximate λ_m we calculate E_{N+m+1} and F_{m+1} from Eqs. (B3) and (B5) followed by the calculation of G_{m+1} according to Eq. (B6). If $G_{m+1}>0$, we increase the initial λ_m. If $G_{m+1}<0$, we decrease it. We continue this until we find a λ_m value which gives $G_{m+1}=0$ within the tolerance preset. For a given κ we can find the initial λ_m as follows: When κ is smaller than 5, Eq. (A10) is quite good. We gradually increase κ and find approximate λ_m by extrapolating the λ_m values already determined for smaller κ's.

To calculate the coefficients a_1^m, a_2^m, ... with the resultant λ_m we first obtain u_l using Eqs. (B3) for $l>m$ and Eq. (B4) for $l<m$, respectively, and then obtain the coefficients using Eq. (B2). In this way we can avoid heavy cancellations which might occur if we use the recurrence relation given by Eq. (33) directly. We

normalize these coefficients according to Eq. (25). We fix sign of the coefficients using the facts that

$$C_{-2}^{m}(0,\kappa) \geq 0 \text{ or } \sum_{n\geq 1} a_n^m > 0 \,. \tag{B7}$$

In the above method of calculating λ_m the error caused by truncating terms corresponding to higher than the maximum index $N+m+1$ in Eq. (B3) is of the order of

$$(-)^{N+m-1} u_{N+m+1} \prod_{j=0}^{N+m-2} u_{j+2}^2 \,.$$

We have choosen $N=100$. Computations have been carried out using a CDC 6400 computer at Temple University.

*This work was supported by the U. S. Army Research Office under Grant No. DAAG29-76-G-0040.

[1]P. Debye, *Polar Molecules* (Dover, New York, 1947).

[2]G. Pfister, M. Abkowitz, and R. G. Crystal, J. Appl. Phys. 44, 2064 (1973): J. G. Bergman, J. H. McFee, and G. R. Crane, Appl. Phys. Lett. 18, 203 (1971): B. K. Oh, A. I. Baise, R. E. Salomon, and M. M. Labes, "A Study of the Mechanism of Pyroelectricity in Polymer Films" Night Vision Laboratory, U. S. Army Mobility Equipment Res. Center, Fort Belvoir, VA, Contract No. DAAK02-74-C-0113, January, 1975.

[3]J. B. Lando, H. G. Olf, and A. Peterlin, J. Polymer Sci. 4, 941 (1966): W. W. Doll and J. B. Lando, J. Macromol. Sci. Phys. 4(2), 309 (1970): N. Murayama, Microsymp. Electrical Properties Polym., Tokyo, Japan, January, 1972 (1973).

[4]J. I. Laurentzin, Jr. and R. Zwanzig, Adv. Mol. Relax. Proc. 5, 339 (1973).

[5]J. Frenkel, *Kinetic Theory of Liquids* (Dover, New York, 1955), p. 278.

[6]E. T. Whittaker and G. N. Watson, *A Course of Modern Analysis* (Cambridge U. P. London, 1927), Chap. 17.

[7]E. T. Whittaker, Proc. Edinburgh Math. Soc. 33, 14 (1914–1915).

[8]E. L. Ince, Proc. Math. Soc. London (2) 23, 56 (1923).

[9]F. M. Arscott *Periodic Differential Equations* (McMillan, New York, 1964), Chap. 7.

[10]S. Goldstein, Trans. Philos. Soc. Cambridge 23, 303 (1927): N. W. McLachlan, *Theory and Application of Mathieu Functions* (Clarendon, Oxford, 1947): Ref. 7, Chap. III.

[11]O. Perron, *Die Lehre von den Kettenbruchen* (Teubner, Stuttgart, Germany, 1957), 3rd ed., Vol. II., Sec. 46.

Space charge, thermal expansion, and pyroelectricity in polymers

R. E. Salomon, H. Lee, C. S. Bak, and M. M. Labes

Department of Chemistry, Temple University, Philadelphia, Pennsylvania 19122
(Received 2 February 1976; in final form 17 May 1976)

The nonlinear thermal expansion of an insulating film containing trapped space charge leads to a reversible pyroelectric current. A general expression for the pyroelectric coefficient of such a system which also includes a contribution from a nonuniform dielectric constant is derived. A simplified expression applicable to insulators with small gradients is also derived and used to make an order-of-magnitude estimate of the pyroelectric coefficient of PVF_2.

PACS numbers: 81.50.Nv, 77.70.+a, 65.70.+y

The role of trapped space charge on the pyroelectric currents observed in polymers such as polyvinylidene fluoride (PVF_2) is difficult to assess although some workers have suggested that trapped charge plays a role in pyroelectricity[1] and piezoelectricity[2] in this material as well as in other polymers.[3] One can show that a uniform thermal expansion of the lattice in the thickness direction in a material containing trapped space charge does not lead to any pyroelectric current even if the space-charge distribution is highly asymmetric.

In the following we shall consider the thermal expansion only in the thickness direction of the thin films which are used in pyroelectric and piezoelectric experiments. To show that a uniform thermal expansion of a material containing frozen space charge, i.e., space charge bound to the lattice or in deep traps does not lead to pyroelectricity, one sets up Poisson's equation and calculates the surface charge density necessary to maintain a vanishing potential difference across the sample. It is found that this surface charge density is invariant to expansions or contractions which do not distort the space charge as long as the potential difference across the sample is maintained at a zero value. Conversely, distortive transformations will indeed lead to pyroelectric currents and if these distortions are thermally reversible, then they will lead to reversible pyroelectric currents of the type observed in PVF_2.[4]

In a previous work[5] we have shown that the finite temperature dependence of the quadratic electrostriction does lead to a finite reversible pyroelectric current in a homogeneous sample with an asymmetric space-charge distribution. Quadratic electrostriction, although universal, is a rather weak effect,[6] and hence is not expected to be of particular importance in accounting for the rather large pyroelectric coefficients (4×10^{-9}C/cm^2°C) found in PVF_2.[7]

Polymer films, by the very nature of their fabrication, may be expected to be far from homogeneous in their physical properties. Without extensive discussions of the causes of this lack of homogeneity, we temporarily assume that a gradient in various properties may exist across the film. In particular we consider a gradient in both the linear coefficient of thermal expansion and dielectric constant in the thickness direction. Evidence for nonuniformity in other properties of PVF_2, such as the polarization, have previously been reported.[8] We shall now explore the effects that these gradients can have on the reversible pyroelectric activity of material which also contains frozen space charge.

We let x represent position in the film at a reference temperature T_0 and let x' represent the position of the same point in the film after thermal expansion due to the temperature change ΔT. The relation between x' and x is

$$x' = x + \Delta T \int_0^x \alpha(x)\, dx, \tag{1}$$

where $\alpha(x)$ is the linear coefficient of thermal expansion. Using the symbols ϵ, E, and ρ to represent the dielectric constant, electric field, and space-charge density, respectively, we write Poisson's equation in one dimension as

$$\frac{d(\epsilon E)}{dx'} = \rho(x'). \tag{2}$$

The pyroelectric current is typically measured under conditions of zero potential difference across the film and hence

$$\int_0^L E(x')\, dx' = 0, \tag{3}$$

where L is the film thickness at $T = T_0 + \Delta T$. Using the superscript zero to denote conditions at $T = T_0$ we write for the condition of a frozen space charge

$$\rho(x')\, dx' = \rho^0(x)\, dx. \tag{4}$$

In the following we assume ΔT is small and therefore the dielectric constant can be expressed as the sum of a temperature-independent part and a temperature-dependent part which is proportional to ΔT. In passing we note that there is a relation, although not a direct one, between the dielectric constant and the thermal-expansion coefficient. We allow both parts of the dielectric constant to vary with position. We therefore write

$$\epsilon(x') = \epsilon^0(x) + a(x)\Delta T. \tag{5}$$

It is convenient to regard the film at $x = 0$ as fixed in space, i.e., clamped at $x = 0$ only. The variation of the surface charge with time at $x = 0$ can then be taken as the pyroelectric current. At other points we have a coordinate system that moves with temperature and this would complicate the calculation of the displacement

current. We emphasize that the current we consider is entirely displacive in origin. In the subsequent calculation we shall require the quantity $\epsilon_0 E_0$, which for small ΔT may be expressed as

$$\epsilon_0 E_0 = \epsilon_0^0 E_0^0 + \gamma \Delta T, \tag{6}$$

where the subscript zero denotes $x = 0$ and γ is the pyroelectric coefficient. The solution of these equations begins by integrating Eq. (2) between zero and x'. Equations (5) and (6) are then incorporated into the integrated form of Eq. (2) which leads to

$$E = \frac{\epsilon_0^0 E_0^0 + \gamma \Delta T + \int_0^x \rho^0(x)\, dx}{\epsilon^0(x) + a(x)\Delta T}. \tag{7}$$

Noting from Eq. (1) that

$$dx' = dx\,[1 + \alpha(x)\Delta T] \tag{8}$$

we combine Eqs. (3), (4), (7), and (8) and obtain a vanishing power series in ΔT. Setting the constant term and the term linear in ΔT to zero separately, we obtain two new equations. The first is

$$E_0^0 \epsilon_0^0 = -\left(\int_0^{L_0} \frac{1}{\epsilon^0(x)} \int_0^x \rho^0(x)\, dx\, dx\right)\left(\int_0^{L_0} \frac{dx}{\epsilon^0(x)}\right)^{-1} \tag{9}$$

and the second is

$$\gamma = \left(-\int_0^{L_0} \beta(x) \int_0^x \rho^0(x)\, dx + E_0^0 \epsilon_0^0\, dx\right)\left(\int_0^{L_0} \frac{dx}{\epsilon^0(x)}\right)^{-1}, \tag{10}$$

where

$$\beta(x) = \frac{\alpha(x)}{\epsilon^0(x)} - \frac{a(x)}{\epsilon^0(x)^2}. \tag{11}$$

Let us first consider the especially simple case where the dielectric constant is invariant with respect to space and temperature. In this case the pyroelectric coefficient is written

$$\gamma = -\int_0^{L_0} \frac{\alpha(x)}{L_0} \times\left(\int_0^x \rho^0(x)\, dx - \frac{1}{L_0}\int_0^{L_0}\int_0^x \rho^0(x'')\, dx''\, dx\right) dx. \tag{12}$$

From Eq. (12) it is apparent that γ is zero if α is constant in space.

It is of some interest to compare the contributions that ϵ, α, ρ, and their gradients make to the magnitude of the pyroelectric coefficients. A method we use to evaluate these relative contributions is a method of linear variation where the gradients are small. Thus we write

$$\epsilon^0(x) = \epsilon_0^0(1 + \epsilon^* \xi x/L_0), \tag{13}$$

where ξ is a parameter allowed to go from zero (no gradient) to unity (full gradient). $\epsilon_0^0 \epsilon^* \xi/L_0$ is of course the gradient in $\epsilon^0(x)$. The conclusions reached in the following analysis are strictly valid only for the type of gradients described. The corresponding equations for $\alpha(x)$ and $a(x)$ are

$$\alpha(x) = \alpha_0(1 + \alpha^* \xi x/L_0), \qquad a(x) = a_0(1 + a^* \xi x/L_0). \tag{14}$$

Inspection of Eqs. (9) and (10) reveals that γ is linear in ρ and hence, if we express ρ^0 in power-series form, namely,

$$\rho^0 = \sum_{n=0} C_n (x/L_0)^n, \tag{15}$$

then we may evaluate each term and its contribution to the pyroelectric coefficient independently. The result to first order in ξ is

$$\gamma = -\xi L_0\left(\frac{a_0}{\epsilon_0^0}\epsilon^* + \alpha_0 \alpha^* - \frac{a_0 a^*}{\epsilon_0^0}\right)\sum_{n=0} C_n g_n, \tag{16}$$

where

$$g_n = \frac{1}{2(n+2)(n+3)}. \tag{17}$$

For these small gradients Eq. (16) tells us the following. If $\alpha^* = 0$, i.e., no gradient in the coefficient of expansion, then a pyroelectric effect is possible provided that both the dielectric constant is temperature dependent ($a_0 \neq 0$) and that there be a gradient in either the temperature-dependent or temperature-independent part of the dielectric constant. To be noted is the fact that not only the magnitude of the space charge, but its distribution within the film, determines the magnitude of the pyroelectric coefficient. From Eqs. (16) and (17) one sees that a uniform space charge (coupled with linear variations in the dielectric and thermal-expansion constants) leads to a maximum pyroelectric coefficient. Although Eq. (16) suggests that the pyroelectric coefficient should increase with film thickness, the nonuniformity in the space-charge distribution may also increase with increasing film thickness and this could override or simply nullify the advantages of a thicker film.

Because of the large number of attendant assumptions in Eq. (16), we will not attempt a calculation of the pyroelectric coefficient of a poled polymer. In the case of PVF_2, sufficient data are available, however, to permit an order-of-magnitude estimate of γ. The space-charge distribution has not, however, been determined for this material and hence one can only estimate the space charge as of the same order of magnitude as that produced in other insulating polymers. For example, Monteith[9] found trapped-electron densities of the order of $10^{15}/cm^3$ in Mylar irradiated with a nonpenetrating electron beam. Seivatz[10] using a Townsend discharge method produced trapped-electron densities of $10^{16}/cm^3$. Of particular interest here is the finding of a space-charge depth of penetration of a few microns at fields of 10^6 V/cm. A detailed description of the related work on Mylar is given by Creswell and Perlman.[11] In Teflon, on the other hand, Sessler[12] reports trapped-electron densities of the order of $10^{14}/cm^3$. Accordingly we shall take a value of 10^{15} electrons/cm^3 as applicable to strongly poled PVF_2. If we now assume equal gradients in the temperature-dependent and temperature-independent parts of the dielectric constant and further take the change in the thermal-expansion coefficient as 10% from one end of the film to the other, then using the value of 2×10^{-4} T^{-1} as the linear coefficient of thermal expansion,[13] we calculate a pyroelectric coefficient in

a 6-μm film of 1.6×10^{-13} C/cm^2 °C. The assumption of equal gradients in the temperature-dependent and temperature-independent parts of the dielectric constant is not crucial since the entire temperature dependence of the dielectric constant of PVF_2 is only about 10^{-2} °C^{-1}.[14,15]

This estimate of the pyroelectric coefficient of $\sim10^{-13}$ C/cm^2 °C is four orders of magnitude lower than the measured pyroelectric coefficient in PVF_2. We have some experimental indication[16] that the trapped-electron density in PVF_2 may be $\sim10^{17}$/cm^3, and ionic trapped charge might also contribute to the pyroelectric coefficient; nevertheless, it is unlikely that these modifications would lead to a prediction of γ of $>10^{-11}$. Thus a space-charge mechanism seems unlikely unless a peculiar distribution of this charge, or a particularly adventitious case of the more general Eq. (10) is involved.

The more frequently invoked mechanism[17,18] for pyroelectricity in PVF_2 is to attribute it to a spontaneous polarization caused by reorientation of the dipoles associated with C-F bonds. The reorientation is caused by rotation of polymer chains or segments in a strong field at elevated temperatures—the poling process—and the pyroelectric currents are viewed as involving a thermal oscillation of dipoles about a fixed mean position. The lack of direct structural evidence for such changes in orientation, and the form of the pyroelectric current dependence on poling conditions have led to doubt about this mechanism, and implied that trapped charges play some role in the pyroelectric behavior. Murayama *et al.*[19] have concluded that piezoelectricity in PVF_2 *cannot* be attributed to the stress dependence of the polarization but to trapped charges, i.e., that β-form PVF_2 favors trapping as compared to the α form and that the structure is only important to facilitate this trapping function. The relation between space charge and a nonlinear dielectric constant (as in ferroelectric crystals) has previously been discussed.[20]

We have seen in this work that in order for trapped charge to explain pyroelectricity in PVF_2, a special (unknown) space-charge distribution is required. Experiments are underway to elucidate the trapping characteristics of PVF_2, but at this writing, the mechanism (or mechanisms) of pyroelectricity in PVF_2 is not fully understood.

This work was supported by the U.S. Army Research Office under Grant No. DAAG29-76-G-0040.

[1]G. Pfister, M. Abkowitz, and R.G. Crystal, J. Appl. Phys. **44**, 2064 (1973).
[2]T. Furukawa, Y. Uematsu, K. Asakawa, and Y. Wada, J. Appl. Polym. Sci. **12**, 2675 (1968).
[3]A.W. Stephens, A.W. Levine, J. Fech, Jr., T.J. Zreblec, A.V. Cafiero, and A.M. Garofalo, Thin Solid Films **24**, 361 (1974).
[4]H. Burkard and G. Pfister, J. Appl. Phys. **45**, 3360 (1974).
[5]R.E. Salomon, B.K. Oh, and M.M. Labes, J. Chem. Phys. **64**, 3375 (1975).
[6]P.W. Forsburhg, Jr., in *Handbuch der Physik*, edited by S. Flugge (Springer-Verlag, Berlin, 1956), Vol. XXVI.
[7]G.W. Day, C.A. Hamilton, R.L. Peterson, R.J. Phelan, Jr., and L.O. Mullen, Appl. Phys. Lett. **24**, 456 (1974).
[8]R.L. Peterson, G.W. Day, P.M. Gruzensky, and R.J. Phelan, Jr., J. Appl. Phys. **45**, 3296 (1974).
[9]L.K. Monteith, J. Appl. Phys. **37**, 2633 (1966).
[10]H. Selvatz and J.J. Brophy, Ann. Rep. Conf. Electr. Insul. Dielectr. Phenom. **1**, 1356 (1965).
[11]R.A. Creswell and M.M. Perlman, J. Appl. Phys. **41**, 2365 (1970).
[12]G.M. Sessler, J. Appl. Phys. **43**, 405 (1972).
[13]H. Sasabe, S. Saito, M. Asahina, and H. Kakutani, J. Polym. Sci. A-2 **7**, 1405 (1969).
[14]S. Uemura, J. Polym. Sci. **12**, 1179 (1974).
[15]H. Kakutani, J. Polym. Sci. A-2 **8**, 1177 (1970).
[16]H. Lee, C.S. Bak, R.E. Salomon, and M.M. Labes (unpublished).
[17]G. Pfister and M.A. Abkowitz, J. Appl. Phys. **45**, 1001 (1974).
[18]J.H. McFee, J.G. Bergman, and G.R. Crane, Ferroelectrics **3**, 305 (1972).
[19]N. Murayama, T. Oikawa, T. Katto, and K. Nakamura, J. Polym. Sci. Polym. Phys. Ed. **13**, 1033 (1975).
[20]P.E. Bloomfield, I. Lefkowitz, and A.D. Aronoff, Phys. Rev. B **4**, 974 (1971).

On the possibility of pyroelectric currents produced by nonlinear space-charge distributions *

R. E. Salomon, Byung K. Oh, and M. M. Labes

Department of Chemistry, Temple University, Philadelphia, Pennsylvania 19122
(Received 21 July 1975; in final form 16 October 1975)

The inhomogeneous electric field in an insulator containing fixed space charges leads to electrostriction. This electrostriction is temperature dependent and as a result a temperature change causes a distortion of the charge distribution which then leads to a pyroelectric current. This current is calculated in terms of the charge distribution and temperature coefficient of the quadratic electrostriction constant.

PACS numbers: 77.70., 78.20.H, 85.50.L, 77.60.

Solids containing immobile or deeply trapped space charge have a rather widespread occurrence.[1] The concentration of charge required to affect the electrical properties of such systems is extremely low; furthermore, the direct determination of such space charge is a difficult task, particularly when this charge is not readily released by thermal means. It is of interest, therefore, to develop nondestructive means to demonstrate the existence of space charge of either ionic or electronic origin.

One experiment directed towards this goal is the measurement of the reversible pyroelectric current produced when samples are heated or cooled at a uniform rate. The experiment consists of measuring the current under short-circuit conditions (i.e., zero potential difference between electrodes applied to either side of a flat sample). Although the experiment is direct, the interpretation of the results is not. The spatial redistribution of space charge which accompanies ordinary (linear) thermal expansion does not produce any current in the external circuit. This can be demonstrated theoretically by applying the boundary conditions (zero potential difference between the electrodes and electroneutrality) to the solution of Poisson's equation for the problem. The surface charge density and hence the current is invariant to a simple linear expansion. The related problem wherein there is a spatial redistribution among the traps has been treated elsewhere.[2,3]

On the other hand, nonlinear expansions or contractions of the lattice can produce a pyroelectric current. This current is a displacement current and occurs even with blocking electrodes. Such transformations, rather than simply enlarging or contracting the distribution, distort it. Such a distortion of the lattice occurs in the phenomenon of electrostriction. We consider in particular the phenomenon of quadratic electrostriction which, unlike linear electrostriction, is characteristic of all materials and we specifically exclude ferroelectric materials from consideration. Related treatments dealing with space-charge distributions in ferroelectrics are described elsewhere.[4,5] A definition of quadratic electrostriction can be made by relating the length of some kth region of a flat film λ_k, in the presence of a field E_k, to the length λ_0 of the same region in the absence of a field. The relation is

$$\lambda_k = \lambda_0(1 + \Omega E_k^2), \tag{1}$$

where Ω is the quadratic electrostriction constant.[6,7] As applied to the problem under consideration, the inhomogeneous field arises from the space charge itself. The distortion of the lattice as a result of temperature variation comes about through the temperature dependence of Ω. Consider a film of thickness L, dielectric constant ϵ, and space-charge distribution $\rho^0(x)$ for $0 \le x \le L$ with $\Omega = 0$. Imagine the film to be divided into m regions of length $\lambda_0 = L/m$ with space charge $\rho^0(k)$, $1 \le k \le m$, in the kth region. The quadratic electrostriction constant is now allowed to attain its true value, Ω; because of electrostriction the length of the kth region is transformed from λ_0 to λ_k and ρ_k^0 becomes ρ_k. Poisson's equation and the boundary conditions of zero potential difference and electroneutrality lead respectively to the equations

$$E_{k+1} - E_k = \rho_k \lambda_k/\epsilon, \tag{2}$$

$$\sum_1^m E_k \lambda_k = 0, \tag{3}$$

$$\rho_k \lambda_k = \rho_k^0 \lambda_0. \tag{4}$$

By combining Eqs. (2) and (4) one obtains

$$E_k = E_0 + \lambda_0 \sum_1^k \rho_i^0/\epsilon, \tag{5}$$

where E_0 is the field at $x = 0$. By substituting Eqs. (1) and (5) into Eq. (3) we obtain

$$0 = m(E_0 + E_0^3\Omega) + (1 + 3\Omega E_0^2)\sum_1^m \lambda_0 \sum_1^k (\rho_i^0/\epsilon) + \Omega \sum_1^m \lambda_0^3 \left(\sum_1^k (\rho_i^0/\epsilon)\right)^3 + 3E_0\Omega \sum_1^m \lambda_0^2 \left(\sum_1^k (\rho_i^0/\epsilon)^2\right). \tag{6}$$

To find E_0 in terms of Ω we expand E_0 about $\Omega = 0$.

$$E_0 = \gamma_0 + \gamma_1\Omega + \cdots + \gamma_n\Omega^n + \cdots. \tag{7}$$

Combining Eqs. (6) and (7) one obtains

$$E_0 = -a + \Omega(3ab - 2a^3 - c) + \cdots, \tag{8}$$

where

$$a = (1/m)\sum_1^m \lambda_0 \sum_1^k \rho_i^0/\epsilon = (1/m)\int_0^m \left\{\int_0^{kL/m} [\rho^0(x)/\epsilon]\,dx\right\} dk, \tag{9}$$

$$b = (1/m)\sum_1^m \lambda_0^2 \left(\sum_1^k \rho_i^0/\epsilon\right)^2 = (1/m)\int_0^m \left\{\int_0^{kL/m} [\rho^0(x)/\epsilon]\,dx\right\}^2 dk, \tag{10}$$

$$c=(1/m)\sum_{1}^{m}\lambda_0^3\left(\sum_{1}^{k}\rho_i^0/\epsilon\right)^3$$

$$=(1/m)\left\{\int_0^{kL/m}[\rho^0(x)/\epsilon]dx\right\}^3 dk. \tag{11}$$

As an example of this result, consider a simple monomonial distribution given as

$$\rho^0(x)=A_n x^n \tag{12}$$

with

$$\int_0^L \rho^0(x)\,dx=Q$$

$$=A_n L^{n+1}/(n+1). \tag{13}$$

In this manner, one has the same total space charge for all n. A_n is given as

$$A_n=Q(n+1)/L^{n+1}. \tag{14}$$

As applied to Eqs. (9)–(11) we find

$$\epsilon a=\frac{Q}{n+2},\quad \epsilon b=\frac{Q^2}{2n+3},\quad \text{and}\quad \epsilon c=\frac{Q^3}{3n+4}. \tag{15}$$

The pyroelectric coefficient, p, associated with this distribution is given as

$$p=i\left(\frac{dT}{dt}\right)^{-1}=\epsilon\left(\frac{dE_Q}{dt}\right)\left(\frac{dT}{dt}\right)^{-1}$$

$$=\epsilon^{-2}\frac{d\Omega}{dT}\,Q^3\left(\frac{3}{(n+2)(2n+3)}-\frac{2}{(n+2)^3}-\frac{1}{(3n+4)}\right), \tag{16}$$

where i is the current density.

Independent measurements of p, ϵ, and $d\Omega/dT$ leave the two unknown quantities Q, the total charge, and n, the exponent of the distribution. If Q can be determined by releasing all the space charge, the two measurements can be combined to give the distribution. It is clear that p is zero for $n=0$ (a constant space charge and hence no asymmetry in the system) and for $n=0$, which amounts to a simple charge double layer. The optimum is found numerically to be about 3.5.

We note the possibility that insulating dielectrics intended for space applications, which contain space charge produced by ionizing radiation, may produce spurious currents due to electrostriction during thermal changes. We are unaware of any previous experimental work to which Eq. (16) can be applied. All pyroelectric measurements to date have been made with materials that show linear electrostriction.

*Work supported by the U.S. Army Research Office under Grant No. DAAG29-76-0040.

[1]B. Gross, *Charge Storage in Dielectrics* (Elsevier, New York, 1964).
[2]L. K. Monteith and J. R. Hauser, J. Appl. Phys. 38, 5355 (1967).
[3]M. A. Lampert and Peter Mark, *Current Injection in Solids* (Academic, New York, 1970).
[4]I. Lefkowitz, Nature 198, 657 (1963).
[5]P. E. Bloomfield, I. Lefkowitz, and A. D. Aaronoff, Phys. Rev. B 4, 974 (1971).
[6]P. W. Forsburgh, Jr., in *Handbuch der Physik*, edited by S. Flugge (Springer-Verlag, Berlin, 1956), Vol. XXVI.
[7]I. S. Zheludev, *Physics of Crystalline Dielectrics*, *Vol.* 2 (Plenum, New York, 1971).

Reprinted from **MACROMOLECULES**, Vol. 11, Page 171, January-February 1978

Pyroelectricity in Polymer Blends of Poly(vinylidene fluoride)

H. Lee, R. E. Salomon, and M. M. Labes*

Department of Chemistry, Temple University, Philadelphia, Pennsylvania 19122.
Received August 31, 1977

ABSTRACT: Polymer blends of poly(vinylidene fluoride) with both poly(methyl methacrylate) and poly(vinyl fluoride) were prepared and evaluated for pyroelectric activity. Percent crystallinity and extent of α, β, γ, and amorphous phases were evaluated by both x-ray diffraction and infrared spectroscopy. The correlations observed are supportive of a dipole-reorientation model for pyroelectricity.

Pyro- and piezoelectricity in poly(vinylidene fluoride) (PVF_2) are thought to be due to the existence of an oriented dipolar structure induced by "poling" polymer films in a high dc field ("dipole-reorientation" model),[1-5] or to the existence of a nonhomogeneous space charge distribution ("space-charge" model),[6-10] or both phenomena superimposed.[11,12] The purpose of this study was to vary the crystallinity and phases of PVF_2 by blending it with poly(vinyl fluoride) (PVF) and poly(methyl methacrylate) (PMMA) and attempt to correlate pyroelectric behavior with the extent of crystalline phase present. If such a correlation exists, it would be hard to rationalize it in terms of a space-charge model, i.e., further credence would be added to the dipole-reorientation model.

Morphological studies[13-19] have shown that there are three crystalline forms of PVF_2. The α form (form II) has the trans-gauche-trans-gauche' configuration[16] and the β form (form I) has the planar zigzag conformation.[19] The structure of the γ form (form III) is not established. However, there are

0024-9297/78/2211-0171$01.00/0

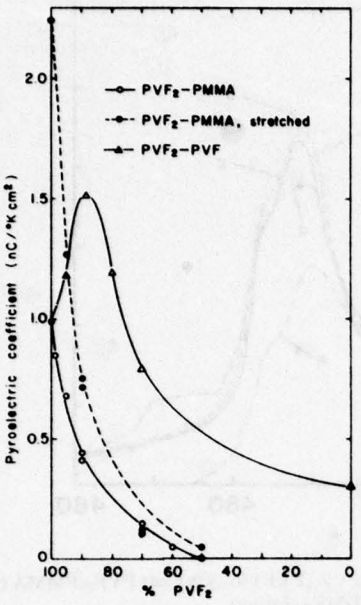

Figure 1. Change in pyroelectric coefficients of polymer blends with change in their composition.

some reports[13,17,20] claiming that the γ form is very similar to the β form. The $-CF_2-$ group of the monomer unit has a dipole moment of 2.1 D.[4] The β form contains two parallel chains and two monomer units per unit cell[19] with a net polarization of 1.3×10^5 C cm^{-2}.[4] The α form contains two antiparallel chains and four monomer units[6] per unit cell. The average dipole moment per monomer unit in the individual α chains is approximately half of that in the β chains, but the net polarization in the α phase is zero due to the antiparallelism of the chains.

The fraction of the planar zigzag form can be increased (about 50%) by stretching the film,[19,21,22] by crystallization from dimethyl sulfoxide solution,[23] or by crystallization from the melt under high pressure.[15,21] The crystallinity of PVF_2 can also be changed by making blends with other polymers. PMMA is compatible with PVF_2 and the crystallinity of PVF_2 in this mixture decreases as the fraction of PMMA increases.[24,25] On the other hand, blending with PVF increases the crystallinity of PVF_2, especially of the planar zigzag forms.[26]

Experimental Section

Films of polymer blends were cast from hot solutions of the blends in *N,N*-dimethylformamide (DMF). The concentrations were approximately 15% for PVF_2/PMMA blends and 3–15% for PVF_2/PVF blends. Number average molecular weights of PVF_2, PVF, and PMMA were 120 000, 87 500, and 24 250, respectively. In forming a film, the solution was first spread uniformly on a glass plate using a Gardner Ultra Applicator and dried in an air oven at 110 °C for 30 min. This was followed by subsequent heating at 200 °C for approximately 30 min, which reduced the roughness of the surface. Such an annealing procedure was found necessary to prevent electrical breakdown during subsequent poling. The thickness of the films obtained was typically 20–25 μm for PVF_2/PMMA and 5–15 μm for PVF_2/PVF. Nichrome electrodes of 1.26 cm^2 area were vacuum evaporated onto both sides of the films, and electrical leads were attached to the electrodes using conducting epoxy adhesive (Acme

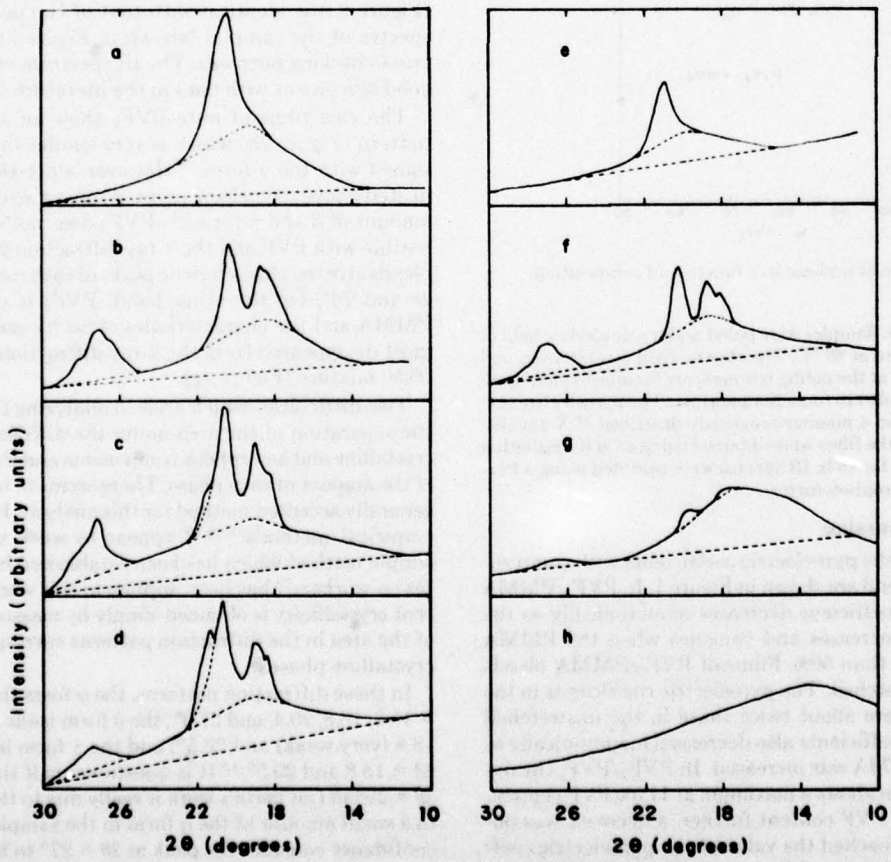

Figure 2. X-ray diffraction intensity patterns of the polymer films: (a) β-PVF_2; (b) PVF_2; (c) PVF_2/PVF (88.5–11.5%); (d) PVF_2/PVF (70–30%); (e) PVF; (f) PVF_2/PMMA (90–10%); (g) PVF_2/PMMA (50–50%); (h) PMMA. All films were heated at 200 °C for 30 min after casting from DMF solutions, with the exception of (a) which was crystallized from dimethyl sulfoxide solution.

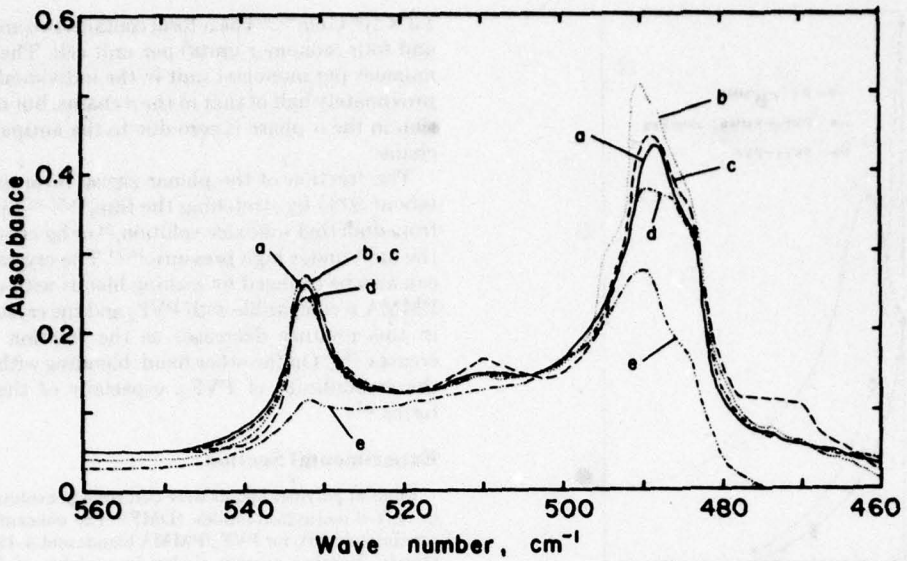

Figure 3. IR spectra of the polymer films: (a) PVF_2; (b) PVF_2/PVF (88.5–11.5%); (c) PVF_2/PVF (70–30%); (d) PVF_2/PMMA (90–10%); (e) PVF_2/PMMA (50–50%). All films were heated at 200 °C for 30 min after casting from DMF solutions.

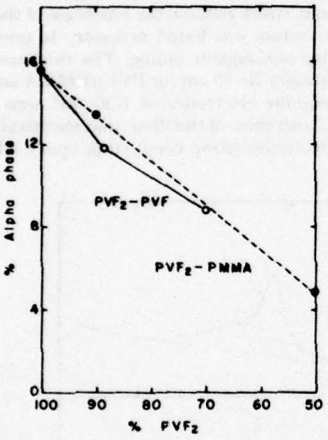

Figure 4. Proportion of α phase as a function of composition.

Chemicals No. 3021). Samples were poled under a dc electric field of 10^6 V cm^{-1} for 30 min at 80 °C. The electric field was removed and the sample was kept at the poling temperature for approximately 15 min before it was cooled to room temperature. The pyroelectric current was measured in a manner previously described.[27] X-ray diffraction patterns of the films were obtained using a Cu Kα radiation at 40 kV and 18 mA for 15 h. IR spectra were recorded using a Perkin-Elmer 225 spectrophotometer.

Results and Discussion

The changes of the pyroelectric coefficients with composition of polymer blend are shown in Figure 1. In PVF_2/PMMA the pyroelectric coefficient decreases monotonically as the PMMA content increases and vanishes when the PMMA content is greater than 50%. Films of PVF_2/PMMA blends could be easily stretched. The pyroelectric coefficients in the stretched films were about twice those in the unstretched films, and these coefficients also decreased monotonically as the content of PMMA was increased. In PVF_2/PVF, the pyroelectric coefficient shows a maximum at 11.5% PVF content. On increasing the PVF content further, a decrease was observed which approached the value of the pyroelectric coefficient in pure PVF, 0.30 nC K^{-1} cm^{-2}. The PVF_2/PVF films were relatively brittle and all attempts to stretch them were unsuccessful.

X-ray diffraction patterns of pure polymers and their blends with other polymers are shown in Figure 2. Although many papers[13-19,21,23,28] have been published concerning polymorphism in PVF_2, the actual designation of the β and γ forms varies from author to author. Gal'perin et al.[18] reported characteristic x-ray diffraction patterns for each form of PVF_2, and the x-ray diffraction pattern of our β-PVF_2 (Figure 2a) is identical with that of Gal'perin's β form. IR spectra of the samples (shown in Figure 3) were taken for cross-checking purposes. The IR spectrum of our β form is in good agreement with data in the literature.[13,17,23]

The cast films of pure PVF_2 show an x-ray diffraction pattern (Figure 2b) which is very similar to the pattern obtained with the α form.[18] However, since the film has been heated above its melting point, it must also contain a certain amount of β and γ forms.[17] PVF_2 does not seem to be compatible with PVF and the x-ray diffraction patterns of these blends give the characteristic peaks of each component (Figure 2c and 2d). On the other hand, PVF_2 is compatible with PMMA and the characteristics of each component have almost disappeared from the x-ray diffraction patterns of the 50:50 mixture (Figure 2g).

Two difficulties which arise in analyzing the data concern the separation of the area under the diffraction curves into crystalline and amorphous components and the determination of the amount of each phase. There seems to be no unique and generally accepted method for this analysis. However, several empirical methods[18,28,29] appear to work satisfactorily. A simple method which has been established by Gal'perin and his co-workers[18] has been applied in this work, in which percent crystallinity is obtained simply by measuring the percent of the area in the diffraction patterns corresponding to each crystalline phase.

In these diffraction patterns, the α form shows peaks at 2θ = 18.2, 18.8, 20.4, and 27.0°; the β form leads to peaks at 2θ = 18.8 (very weak) and 20.5°; and the γ form leads to peaks at 2θ = 18.8 and 20.5°.[18] It is questionable if the small peak at 2θ = 27° in Gal'perin's work is really due to the γ form or due to a small amount of the α form in the sample. We may with confidence consider the peak at 2θ = 27° to be purely due to the α form. The relative area of the α peak, S_α, is plotted as a function of composition in Figure 4. Since the peaks in the range of 2θ = 17 to 21° are due to all three of these forms, we

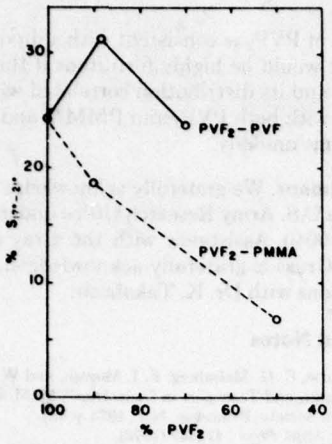

Figure 5. Change of $S_{17\text{-}21°}$ with composition.

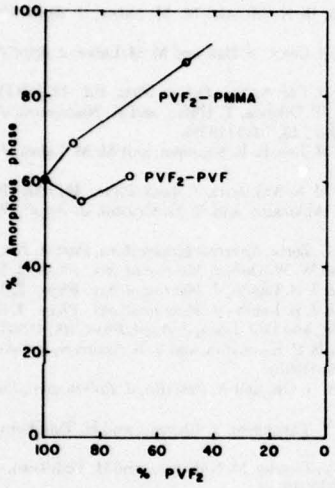

Figure 6. Proportion of amorphous phase as function of composition.

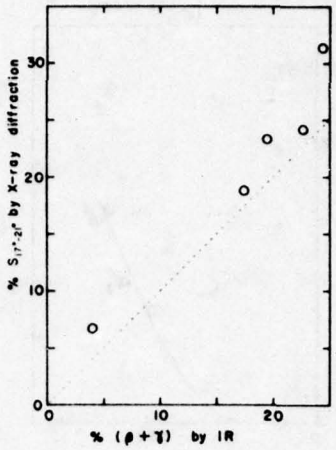

Figure 7. Comparison of $S_{17\text{-}21°}$ and percent $(\beta + \gamma)$ obtained from IR spectra.

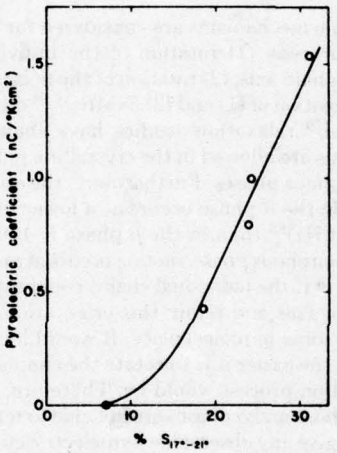

Figure 8. Correlation between pyroelectric coefficient and $S_{17\text{-}21°}$.

can not consider them separately. The change of the relative peak area, $S_{17°\text{-}21°}$, with composition is shown in Figure 5.

In the PVF_2/PMMA blends, the amount of amorphous phase increases almost linearly with the PMMA content (Figure 6), while at the same time the amount of the crystalline phases decreases (Figures 4 and 5) and at 50% PMMA, the sample becomes almost completely amorphous (Figure 6). In PVF_2/PVF blends, the amount of amorphous phase stays more or less at a constant level (Figure 6). However, the amount of the α phase decreases as the PVF content increases (Figure 4). It is interesting to note that the relative peak area in the range of $2\theta = 17$ to 21°, $S_{17\text{-}21°}$, shows a maximum at 11.5% of PVF content (Figure 5).

A similar change is observed in the IR spectra (Figure 3). The peaks at 532 and 510 cm^{-1} are due to the α and β forms, respectively.[13,17,23] All the IR spectra were normalized for the same amount of pure PVF_2 per unit area (1 mg of PVF_2 cm^{-2}). The α peak at 532 cm^{-1} is relatively well separated from other peaks. Absorption by the 50–50 mixture of PVF_2/PMMA (Figure 3e) is similar to the absorption by molten PVF_2[31,32] and is therefore assumed to be due to the amorphous phase. The peak at 510 cm^{-1} is considered to be due to absorption by β and amorphous phases. The absorption around 490 cm^{-1} is due to overlap of several different absorptions. Most of the absorption by the γ phase and some by the amorphous phase appears around 490 cm^{-1}.[13,31,32] It is interesting to note that the amount of β phase seems to increase largely at the expense of the γ phase (Figures 3b and 3c). The peak height of the IR spectra was calibrated with respect to the x-ray diffraction data. The percent crystallinity of $(\beta + \gamma)$ obtained in this way shows good agreement with that from x-ray diffraction data (Figure 7).

Since the amount of the α and amorphous phases is not closely correlated with the pyroelectric coefficients, it may be inferred that these phases are not pyroelectric. On the other hand, $S_{17\text{-}21°}$ changes in a fashion similar to the change in the pyroelectric coefficient as the composition changes. Since $S_{17\text{-}21°}$ represents the amount of crystalline phase and the α phase is already known to be nonpyroelectric, the pyroelectricity is mainly due to the β and γ phases. The relationship between the pyroelectric coefficient and $S_{17\text{-}21°}$ is shown in Figure 8. A similar correlation is obtained between the pyroelectric coefficient and the percent $(\beta + \gamma)$ estimated by IR spectroscopy (Figure 9).

Consequently the pyroelectricity in PVF_2 is mainly attributed to the β and γ phases and the contribution by the α and amorphous phases is negligible. This fact strongly supports the dipole-reorientation mechanism for pyroelectricity in PVF_2. It is not possible to determine the differences in activity between β and γ phases, and since these two phases have similar structures, they might be expected to have comparable pyroelectric activity.

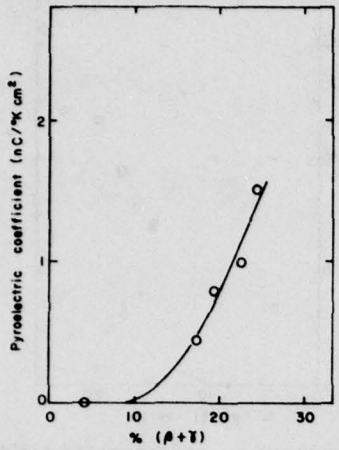

Figure 9. Correlation between pyroelectric coefficient and percent ($\beta + \gamma$) phases as determined by IR method.

Three possible mechanisms are considered for the dipole-reorientation process: (1) rotation of the individual chain around its own chain axis; (2) rotation of the polar domains;[30] and (3) a combination of (1) and (2). NMR,[33-35] dielectric,[34-38] and mechanical[39] relaxation studies have shown that restricted rotations are allowed in the crystalline phases as well as in the amorphous phases. Furthermore, the onset of rotational motion in the α phase occurs at a lower temperature (~70 °C at 110 Hz)[35] than in the β phase (~110 °C at 110 Hz).[35] In the amorphous phase, motion occurs at an even lower temperature.[33-35] If the individual chains could rotate around their own chain axes and retain this orientation, then they should exhibit some pyroelectricity. It would be reasonable to assume that the easier it is to rotate the chains, the faster the depolarization process would be. Therefore, we suggest that the amorphous and α phases are not able to retain enough polarization to give any observable pyroelectric current in the second heating cycle.

The crystalline phases are of course dispersed in the amorphous phase and the polymer chains extend into the amorphous phase. Since the amorphous phase is relatively fluid at temperatures well above the glass-transition temperature of the polymer, partial rotation of the polar domains can be expected. In uniaxially stretched PVF_2, the remanent polarization at room temperature is about 4×10^{-3} C cm^{-2}.[5] This is equivalent to about 3% orientation assuming pure β phase for the uniaxially stretched film. In the PVF_2/PMMA blends, the pyroelectricity becomes zero before $S_{17-21°}$ becomes zero (Figure 8). This fact may be explained as follows. When the percent PMMA increases, the formation of α phase is favored over the formation of other crystalline phases, and the fraction of the pyroelectric phases becomes proportionately smaller. At the same time only a small amount of PVF_2 can crystallize so that the average size of crystalline domains becomes very small. Accordingly, the torque exerted on the polar crystallites is too small to align them along the direction of the applied electric field.

In conclusion, the correlations observed between pyroelectric activity and percent of $\beta + \gamma$ crystalline phases in polymer blends of PVF_2 is consistent with a dipole reorientation model. It would be highly fortuitous if the extent of trapped charge and its distribution correlated with crystallinity in blends with both PVF_2 and PMMA, and this letter explanation seems unlikely.

Acknowledgment. We gratefully acknowledge support of this work by the U.S. Army Research Office under Grant No. DAAG29-76-G-0040. Assistance with the x-ray diffraction data by Dr. L. Gruss is gratefully acknowledged, as well as helpful discussions with Dr. K. Takahashi.

References and Notes

(1) M. G. Broadhurst, C. G. Malmberg, F. I. Mopsik, and W. P. Harris in "Electrets, Charge, and Transport in Dielectrics", M. M. Perlman, Ed., Electrochemical Society, Princeton, N.J., 1973, p 492.
(2) H. Ohigashi, *J. Appl. Phys.*, **47**, 949 (1976).
(3) Y. Wada and R. Hayakawa, *Jpn. J. Appl. Phys.*, **15**, 2041 (1976).
(4) K. Nakamura and Y. Wada, *J. Polym. Sci., Part A-2*, **9**, 161 (1971).
(5) M. Tamura, S. Hagiwara, S. Matsumoto, and N. Ono, *J. Appl. Phys.*, **48**, 513 (1977).
(6) R. E. Salomon, B. K. Oh, and M. M. Labes, *J. Appl. Phys.*, **47**, 1710 (1976).
(7) R. E. Salomon, H. Lee, C. S. Bak, and M. M. Labes, *J. Appl. Phys.*, **47**, 4206 (1976).
(8) N. Murayama, *J. Polym. Sci., Polym. Phys. Ed.*, **13**, 929 (1975).
(9) N. Murayama, T. Oikawa, T. Katto, and K. Nakamura, *J. Polym. Sci., Polym. Phys. Ed.*, **13**, 1033 (1975).
(10) K. Takahashi, H. Lee, R. E. Salomon, and M. M. Labes, *J. Appl. Phys.*, **48**, 4694 (1977).
(11) G. Pfister and M. A. Abkowitz, *J. Appl. Phys.*, **45**, 1001 (1974).
(12) G. Pfister, M. Abkowitz, and R. G. Crystal, *J. Appl. Phys.*, **44**, 2064 (1973).
(13) G. Cortili and G. Zerbi, *Spectrochimica Acta, Part A*, *23a*, 2216 (1967).
(14) J. B. Lando and W. W. Doll, *J. Macromol. Sci., Phys.*, **2**, 205 (1968).
(15) W. W. Doll and J. B. Lando, *J. Macromol. Sci., Phys.*, **2**, 219 (1968).
(16) W. W. Doll and J. B. Lando, *J. Macromol. Sci., Phys.*, **4**, 309 (9170).
(17) W. M. Prest, Jr., and D. J. Luca, *J. Appl. Phys.*, **46**, 4136 (1975).
(18) Y. L. Gal'perin, B. P. Kosmynin, and V. K. Smirnov, *Vysokomol. Soedin., Ser. A*, **12**, 1880 (1970).
(19) J. B. Lando, H. G. Olf, and A. Peterlin, *J. Polym. Sci., Part A-1*, **4**, 941 (1966).
(20) R. Hasegawa, Y. Takahashi, Y. Chatani, and H. Tadokoro, *Polym. J.*, **3**, 600 (1972).
(21) R. Hasegawa, Y. Tanabe, M. Kobayshi, and H. Tadokoro, *J. Polym. Sci., Part A-2*, **8**, 1073 (1970).
(22) J. P. Luongo, *J. Polym. Sci., Part A-2*, **10**, 1119 (1972).
(23) K. Okuda, T. Yoshida, M. Sugita, and M. Asahina, *Polym. Lett.*, **5**, 465 (1967).
(24) T. Nishi and T. T. Wang, *Macromolecules*, **8**, 909 (1976).
(25) J. S. Noland, N. N.-C. Hsu, R. Saxon, and J. M. Schmitt, *Adv. Chem. Ser., No.* **99**, 15 (1971).
(26) G. Natta, G. Allegra, I. W. Bassi, D. Sianesi, G. Caporiccio, and E. Torti, *J. Polym. Sci., Part A*, **3**, 4263 (1965).
(27) A. I. Baise, H. Lee, B. Oh, R. E. Salomon, and M. M. Labes, *Appl. Phys. Lett.*, **26**, 428 (1975).
(28) W. W. Doll and J. B. Lando, *J. Macromol. Sci., Phys.*, **4**, 897 (1970).
(29) G. Challa, P. H. Herman, and A. Weidinger, *Makromol. Chem.* **56**, 169 (1962).
(30) B. K. Oh, M. M. Labes, and R. E. Salomon, *J. Chem. Phys.*, **64**, 3375 (1976).
(31) S. Enomoto, Y. Kawai, and M. Sugita, *J. Polym. Sci., Part A-2*, **6**, 861 (1968).
(32) G. Cortili and G. Zerbi, *Spectrochim. Acta, Part A*, **23**, 285 (1967).
(33) V. J. McBrierty, D. C. Douglass, and T. A. Weber, *J. Polym. Sci., Polym. Phys. Ed.*, **14**, 1271 (1976).
(34) H. Sasabe, S. Saito, M. Asahina, and H. Kakutani, *J. Polym. Sci., Part A-2*, **7**, 1405 (1969).
(35) H. Kakutani, *J. Polym. Sci., Part A-2*, **8**, 1177 (1970).
(36) S. Yano, *J. Polym. Sci., Part A-2*, **8**, 1057 (1970).
(37) K. Nakagawa and Y. Ishida, *J. Polym. Sci., Polym. Phys. Ed.*, **11**, 1503 (1973).
(38) A. Peterlin and J. Elwell, *J. Mater. Sci.*, **2**, 1 (1967).
(39) A. Callens, R. De Batist, and L. Eersels, *Nuovo Cimento B*, **33**, 434 (1976).

Nature of injection processes during poling of poly(vinylidene fluoride) and their relationship to pyroelectricity[a)]

K. Takahashi, H. Lee, R. E. Salomon, and M. M. Labes

Department of Chemistry, Temple University, Philadelphia, Pennsylvania 19122
(Received 18 April 1977; accepted for publication 30 June 1977)

By analysis of steady-state current-time-voltage-temperature relationships, it is concluded that a Richardson-Schottky process is dominant at the high fields and temperatures typically employed in poling poly(vinylidene fluoride) to impart pyroelectric and piezoelectric properties. Data on pyroelectric behavior with different layer configurations and with different electrode configurations indicate the primary importance of hole injection.

PACS numbers: 77.70.+a, 77.30.+d, 73.40.Gk, 73.40.Ns

I. INTRODUCTION

Piezoelectric and pyroelectric effects in poly (vinylidene fluoride) (PVF_2)[1-3] are most pronounced when the polymer film is "poled" by placing it in a high dc field while the sample is held at a temperature just below its melting point. The magnitude of the polarization is a function of field, temperature, and time, and typically the sample is quenched to room temperature rapidly with the poling field still applied. Three different mechanisms have been invoked to explain the persistent polarization: (1) alignment of C-F dipoles in a crystalline phase (β phase)[4-8]; (2) injection of charges into the film from the electrodes[3,9-12]; (3) a combination of (1) and (2).[13,14] Experimental evidence exists in support of all three mechanisms, and it is extremely difficult to distinguish among them.

The purpose of this study was to focus on the nature of trapped charges in poled PVF_2 by analyzing the steady-state current-time-voltage-temperature relationships. Many studies have been made of electrical conduction at high fields in polymer films. Several possible types of steady-state currents can be observed in an insulating solid: thermal bulk generation of carriers; space-charge-limited currents (SCLC) in solids (with trap, trap-free, or trap-filled limit cases); emission-limited currents such as Richardson-Schottky (RS) field-assisted thermionic injection of carriers from the electrode, or a Poole-Frenkel process. Indeed, these processes have been invoked to explain the high-field behavior of several polymers. For Mylar film, conduction has been interpreted alternately as Schottky emission[15] or a space-charge effect.[16] Richardson-Schottky field-assisted thermionic injection of carriers from metal electrodes modified by the Poole-Frenkel effect has been suggested as the mechanism of conduction in poly (tetrafluorethylene)[17] and poly (*n*-vinylcarbazole).[18]

In this paper, analyses are presented of the steady-state current-time-voltage-temperature relationships in PVF_2 in terms of both SCLC and RS processes. At the lower temperatures and fields employed, the data are consistent with either analysis, but at high fields and temperatures, analysis in terms of the RS equation is preferable. These high field-temperature conditions are typically employed in poling PVF_2, and data on the pyroelectric behavior taken with different electrode configurations indicate that hole injection is an extremely important factor in inducing pyroelectric activity.

II. EXPERIMENTAL

PVF_2 was obtained from Kureha Chemical Co. in the form of stretched 6-μ and unstretched 30-μ sheets. Metal electrodes of Nichrome, gold, or aluminum were vacuum evaporated onto the films. The area of all the metal electrodes was 1.3 cm^2. Electrical leads were attached using conducting epoxy adhesive (Acme Chemicals, No. 3021). For measurements of pyroelectricity, the samples were heated in a microscope hot stage having controlled heating and cooling rates (Mettler Model FP2). The samples were carefully shielded to eliminate electrical interference from the hot stage heating coils. For a first heating cycle, the poled films were heated at 10 °C/min up to 80 °C and kept at 80 °C for 10 min. Thermally stimulated currents were measured during this heating cycle. Then the samples were cooled to room temperature and, in a second heating cycle, the samples were heated at 2 °C/min and pyroelectric currents were measured. Pyroelectric coefficients were calculated at temperatures of 35 °C. A detailed description of this measurement and the subsequent calculation of the pyroelectric coefficient are reported elsewhere.[19]

Layered film experiments were performed on stacked films of PVF_2-Mylar. PVF_2-Mylar (samples A, B, and C) films were made by spraying PVF_2 solution in *N*, *N*-dimethylformamide (~3 g/20 ml) on one side of a piece of Mylar film followed by subsequent drying in an air oven at 100 °C and annealing at 200 °C for 30 min. PVF_2-Nichrome-Mylar (sample D) film was made by vacuum-evaporating a Nichrome electrode on a Mylar film and spraying the PVF_2 solution on the metal. The same heat treatment described above was given to this sample. The poling conditions and the pyroelectric coefficients of the layered polymer films are shown in Table I.

For steady-state conductivity measurements, a PVF_2 sample with gold electrodes was first poled at a field of 1.0×10^6 V cm^{-1} for 10 min at 90 °C. The sample was placed in an aluminum box for electrical shielding, and

[a)]Work supported by the U.S. Army Research Office under Grant No. DAAG29-76-G-0040.

TABLE I. Pyroelectric coefficients at 35 °C for PVF_2-Mylar stacked samples with Nichrome electrodes.

Sample	Configuration and thickness	Poling Voltage[a] (V)	Polarity of PVF_2 layer	Field on PVF_2 layer[b] (V cm^{-1})	Pyroelectric coefficients at 35 °C (nC cm^{-2} K^{-1}) 1st heating cycle Total of two layers	1st heating cycle PVF_2 layer	2nd heating cycle Total of two layers	2nd heating cycle PVF_2 layer
A	PVF_2 - Mylar 0.68 μ 6.3 μ	2000	+	9.4×10^5	0.156	4.50[c]	0.065	2.05[c]
B	PVF_2 - Mylar 0.68 μ 6.3 μ	2000	−	9.4×10^5	0.078	2.27[c]	0.012	0.25[c]
C	PVF_2-Mylar 5.5 μ 6.3 μ	2300	+ (1st)	7.7×10^5	0.550	2.42[c]	0.278	1.22[c]
			− (2nd)	7.7×10^5	0.025	0.11[c]	0.027	0.12[c]
D	PVF_2-NiCr-Mylar 6.8 μ 6.3 μ	2300	+ (1st)	7.3×10^5	...	3.12	0.520	1.67
			− (2nd)	7.3×10^5	...	3.54	0.610	2.08[c]
								1.98
								2.44[c]

[a] All samples poled at 80 °C for 30 min.
[b] Calculated from Eq. (3).
[c] Calculated from Eq. (4).

the assembly was put into a Delta Design 2300 temperature-controlled oven. Measurements were performed in the temperature range 10–90 °C. A Keithley 160 Digital Multimeter with a copper-constantan thermocouple was used to measure the temperature accurately. In the steady-state current measurements, the order of measurement was such that the applied voltage increased and the temperature decreased. A Keithley 610C electrometer was used for the current measurement, and a Hewlett-Packard 7100BM strip-chart recorder was connected to the electrometer.

III. RESULTS

A. Time dependence of the current

A plot of current versus time at a temperature of 90 °C is shown in Fig. 1. A small time dependence was seen over a long-range time scale. Since the change of the current over the long time period was small, and the decaying slope on the plot of log$I$ versus log$t$ was about the same for different fields, the steady-state current was taken as that current observed at about 40 min after the voltage was applied. The steady-state currents as a function of voltage and temperature are shown in Figs. 2–4.

B. SCLC analysis

To determine if the steady-state currents fit a SCLC analysis, the voltage dependence of the steady-state currents is plotted in Fig. 2. Slopes were measured to be 1.5 and 2.6 at 90 and 10 °C, respectively, with the slopes increasing with decreasing temperature. A SCLC should show a dependence on voltage equal to or greater than V^2,[22] and one would expect the slope to increase as the temperature increased, i.e., the opposite of what is in fact observed. Nevertheless, at the lower temperatures, a SCLC analysis is consistent with the data.

C. RS analysis

The RS effect predicts a current-voltage relationship of the form

$$J = AT^2 \exp(-\Phi_s/kT)\exp(\beta_s V^{1/2}) \qquad (1)$$

with

$$\beta_s = \frac{e}{kT}\left(\frac{e}{4\pi\epsilon\epsilon_0 d}\right)^{1/2}, \qquad (2)$$

where J is the current density, A is a constant 120 A/cm^2 °K^2, T is the absolute temperature, e is the electronic charge, V is the voltage, Φ_s is the Schottky electrode barrier, k is Boltzman's constant, d is the film thickness, ϵ is the dielectric constant, and ϵ_0 is the permitivity of free space. The linear behavior of the isotherms in Fig. 3 is in accord with Eq. (1). The slopes were calculated from Fig. 3 and experimental β_s was found to be in the range 0.15–0.26 V$^{-1/2}$. Table II compares theoretical values of β_s for $d = 6$ μ and $\epsilon = 12$ with experimental values at different temperatures. The experimental β_s values were found to be slightly larger than the theoretical values.

The linearity exhibited by the plots in Fig. 4 of logJ/AT^2 versus $1/T$ is also in accord with Eq. (1) and is used to calculate activation energies. The steady-state currents were measured for both heating and cooling cycles. The current reached a steady state within 5 min after changing the temperature. Activation energies

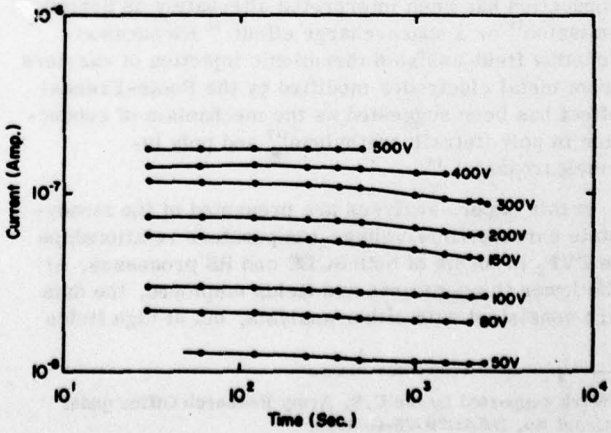

FIG. 1. Log-log plot of current-time relationship at constant voltage for a 6-μ-thick PVF_2 film with Au electrodes at 90 °C.

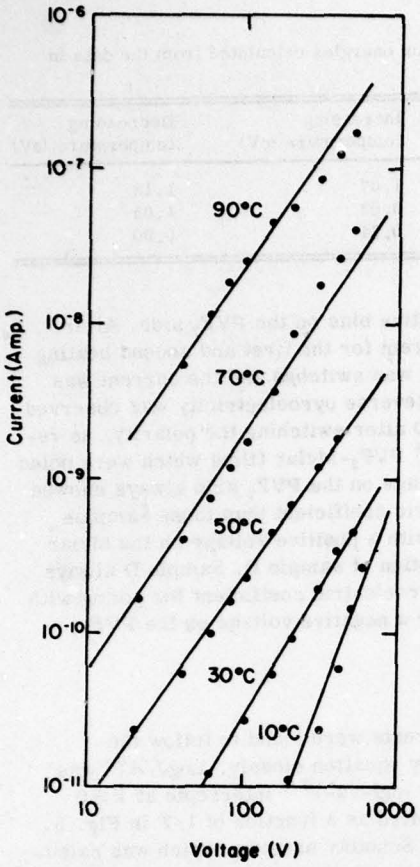

FIG. 2. Log-log plot of current-voltage relationship for a 6-μ-thick PVF_2 film with Au electrodes.

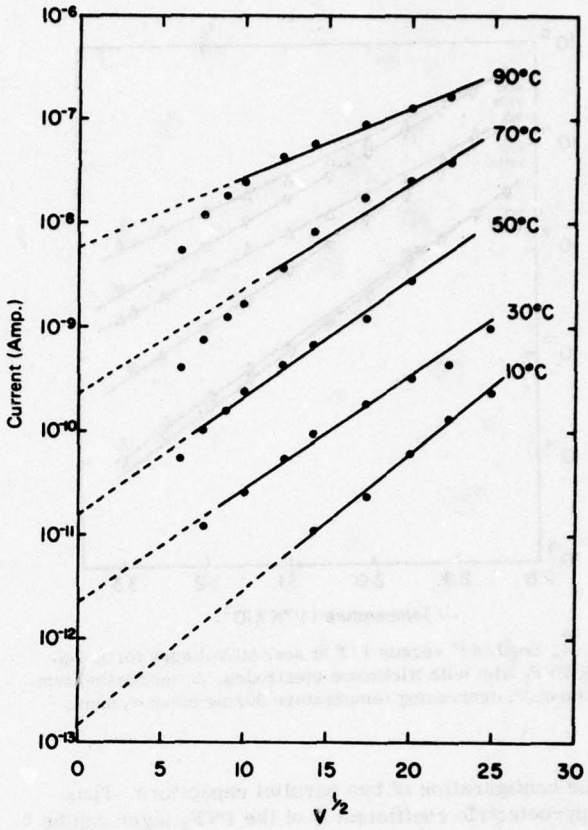

FIG. 3. Log current versus $V^{1/2}$ at various temperatures for a 6-μ-thick PVF_2 film with Au electrodes.

were obtained for these two cycles and are listed in Table III. Currents measured while decreasing the temperature were about the same magnitude as the steady-state currents shown in Fig. 3. The activation energies obtained were considered to be experimental Φ_s values from Eq. (1).

D. Pyroelectricity for PVF_2 films with different electrode configurations

Pyroelectric coefficients of several Au-PVF_2-Al samples were measured. In all cases, a larger pyroelectricity was observed for the sample with the Au electrode positively biased or with the Al electrode negatively biased. The results are shown in Table IV. Pyroelectricity observed with a 6-μ sample in which the Au electrode was positively biased was generally about 30% higher than the case when the Al electrode was positively biased and the pyroelectricity observed with the 30-μ film was 50% higher. The thermally stimulated currents were in all cases more than 10 times larger than the reversible pyroelectric currents.

E. Pyroelectricity for layer configuration films of PVF_2 and Mylar

The results of pyroelectric measurements on PVF_2-Mylar layers are given in Table I. The poling field was calculated from the relation

$$E_1 = \frac{V_0}{d_1 + (\epsilon_1/\epsilon_2)d_2}, \tag{3}$$

assuming parallel-plate capacitor spacings d_1 and d_2 with dielectric constants of ϵ_1 and ϵ_2 for the two dielectrics, respectively. V_0 is the total applied voltage and E_1 is the field on the PVF_2 layer. Values of ϵ_1 and ϵ_2 for PVF_2 and Mylar are 12 and 3.7, respectively. In order to calculate pyroelectric coefficients of the PVF_2 layers, the PVF_2-Mylar films were assumed to be two parallel capacitors. The capacitor which contains charge produced by temperature change in the PVF_2 layer should charge up the other capacitor, the Mylar layer. With this assumption, the measured pyroelectricity for stacked samples is simply due to a charge flow from a charged capacitor to an uncharged capacitor

TABLE II. Comparison of experimental and theoretical β_s values.

Temperature (°K)	β_s (Theor.) ($V^{-1/2}$)	β_s (Expt.) ($V^{-1/2}$)
363	0.144	0.15
353	0.148	0.18
343	0.152	0.23
323	0.162	0.26
303	0.173	0.26
283	0.185	0.26

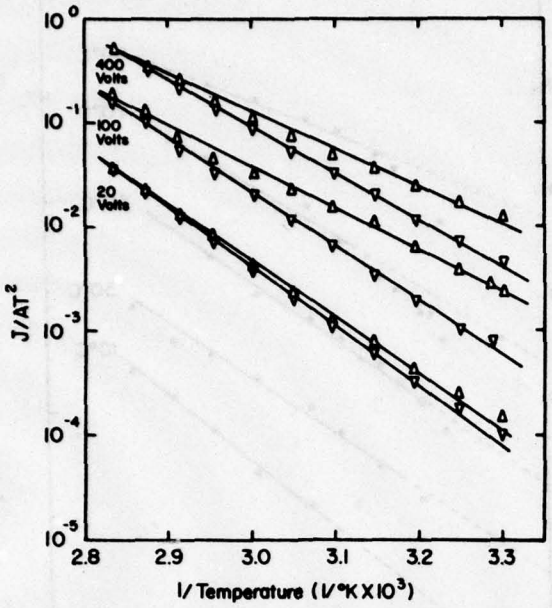

FIG. 4. LogJ/AT^2 versus $1/T$ at several voltages for a 6-μ-thick PVF_2 film with Nichrome electrodes. Δ: increasing temperature; ∇: decreasing temperature during measurement.

in the configuration of two parallel capacitors. Thus, the pyroelectric coefficient Q of the PVF_2 layer can be calculated from the measured pyroelectric coefficient Q' by means of the following equation:

$$Q = \left(1 + \frac{\epsilon_1 d_2}{\epsilon_2 d_1}\right) Q'. \tag{4}$$

For sample D in Table I the directly measured value as well as the calculated value of the pyroelectric coefficient of the PVF_2 layer is given. The calculated values agree with the measured values reasonably well, indicating the validity of Eq. (4).

Samples A and B were made identically, except that sample A was poled with a positive bias on the PVF_2 side, whereas sample B was poled with the positive bias on the Mylar side. Samples C and D were first poled with the positive bias on the PVF_2 side. After measuring the current for the first and second heating cycle, the polarity was switched and the current was again measured. Reverse pyroelectricity was observed in samples C and D after switching the polarity, as reported previously.[5] PVF_2-Mylar films which were poled with a positive voltage on the PVF_2 side always showed a higher pyroelectric coefficient than those samples which were poled with a positive voltage on the Mylar side with the exception of sample D. Sample D always showed a higher pyroelectric coefficient for poling with either a positive or a negative voltage on the PVF_2 side.

TABLE III. Activation energies calculated from the data in Fig. 3.

Applied voltage (V)	Increasing temperature (eV)	Decreasing temperature (eV)
20	1.07	1.13
100	0.80	1.05
400	0.74	0.90

IV. DISCUSSION

Steady-state currents were found to follow the Richardson-Schottky equation closely. LogJ/AT^2 was calculated from the log$I$-vs-$V^{1/2}$ intercepts at $V=0$ from Fig. 3 and plotted as a function of $1/T$ in Fig. 5. The slope gives the Schottky barrier, which was calculated to be about 1 eV. Steady-state current measurements at constant applied voltage of 100 and 400 V gave two different values for the Schottky barrier Φ_s, ~1 and ~0.8 eV, for decreasing temperature and increasing temperature, respectively. The value of ~1 eV for decreasing temperature is consistent with the value obtained from the intercept of the log$I$-vs-$V^{1/2}$ plot of Fig. 5. In the studies of layered films, the largest pyroelectricity was always observed when the PVF_2 film was in contact with the positively biased metal electrode. There is a report[20] that for Mylar films steady-state currents were not limited by Schottky emission but by space charge. Table I shows that Mylar films poled with a positively biased metal electrode

TABLE IV. Pyroelectric coefficients at 35 °C for gold and aluminum electrode configurations. The polarity in the parenthesis indicates the poling polarity on the gold electrode.

Sample	Measurement number[a] 1	2	3	4	Average	Standard deviation
	(nC cm^{-2} K^{-1})					
S-1[b]	(+)1.02	...	...	...		
S-2[b]	(-)0.79	(+)0.98	(-)0.72	...	(+)1.07	0.1424
S-3[b]	(+)1.12	(-)0.60	(+)1.29	...	(-)0.71	0.0785
S-4[b]	(-)0.71	...	...	...		
S-5[b]	(+)0.93	...	...	...		
U-1[c]	(-)0.069	(+)0.162	(-)0.052	...	(+)0.122	0.0344
U-2[c]	(+)0.091	(-)0.060	(+)0.107	...	(-)0.054	0.0115
U-3[c]	(-)0.052	(+)0.157	(-)0.038	(+)0.095		

[a] To repeat the measurement, the sample was heated up to 130 °C for 20 min in order to annihilate previous pyroelectricity.

[b] The 6-μ stretched samples were poled at 1.3×10^6 V cm^{-1} at 25 °C for 8 min.

[c] The 30-μ unstretched samples were poled at 8.0×10^5 V cm^{-1} at 25 °C for 8 min.

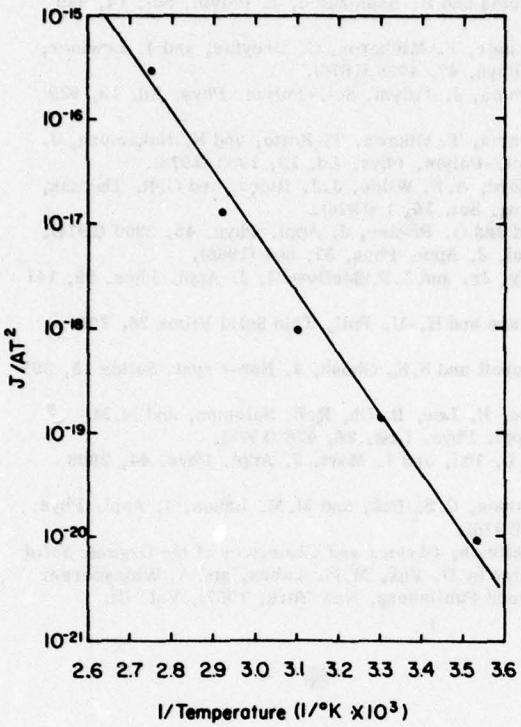

FIG. 5. Log J/AT^2, calculated from the intercepts in Fig. 2, plotted as a function of $1/T$.

were less pyroelectric, which is consistent with less charge injection. The data also show the importance of interfaces between PVF_2 and Mylar and between PVF_2 and Nichrome. One of the possible explanations for this is the occurrence of different values of the Schottky barrier Φ_s at different interfaces, i.e., the Schottky barrier Φ_s for PVF_2-Mylar might be larger than for PVF_2-Nichrome. Hole emission from a positively biased metal electrode into a PVF_2 film seems to occur with samples that are pyroelectrically active, whereas electron emission occurs together with samples that are much less pyroelectrically active.

From measurements of pyroelectricity of PVF_2 films with the different electrodes shown in Table IV, one sees that the ratio of pyroelectricity for the positively biased Au electrode to the positively biased Al electrode was about 0.66 for the 6-μ film and 0.44 for the 30-μ films. These ratios indicate that Richardson-Schottky hole emission is not the sole criteria for the production of pyroelectricity.

Pfister *et al.*[3] also measured current-vs-temperature relationships for various dc fields in PVF_2 (Fig. 11 in Ref. 3). In their results, the relationship of measured currents versus $1/T$ was not linear, and the magnitude of current was larger than that presented in this paper. Indeed, we obtained some results which indicated about the same magnitude of the current level from fresh samples as observed by Pfister *et al.*,[3] but after applying a high field ($\sim 10^6$ V cm^{-1}) at high temperature ($\sim$90 °C) for more than 5 min, the current magnitude was reduced and became reproducible. The reason for this high magnitude of the current for fresh samples may be due to impurity effects associated with trapping. After applying a high field at high temperature, the impurities (probably ionic impurities not originating from defects in the PVF_2 crystalline structure) are swept away to the surface of the polymer film. The difference of the steady-state current measured at increasing and decreasing temperatures in Fig. 3 indicates two different discrete trapping levels.

To determine whether the steady-state currents are emission-limited (a Schottky emission current in this case) or bulk-generated currents (probably a space-charge-limited current), measurements were made of steady-state currents in a PVF_2 film with a gold and an aluminum electrode. The results as shown in Fig. 6 suggest that the steady-state currents are due to electrode effects and not bulk effects, since the currents are clearly different for different metal electrode configurations. When the gold electrode was made positive relative to the aluminum electrode, the current magnitude was about 10 times higher than in the reverse case. This difference indicates that hole emission is more favorable than electron emission, and this is consistent with the results of measurements of pyroelectricity with these two polarities.

This finding suggests that either a hole current enhances pyroelectricity or an electron current militates against pyroelectricity. The latter may be due to space-charge-produced variation in the electric field. However, the currents are so small as to rule out space-charge limitation.[21,22] The hole-electron concept is not entirely appropriate to a tightly bound insulator such as PVF_2. Holes, if they exist, must be highly localized and should serve to weaken hydrogen bonding (H-F) between adjacent polymer chains. We suggest that this

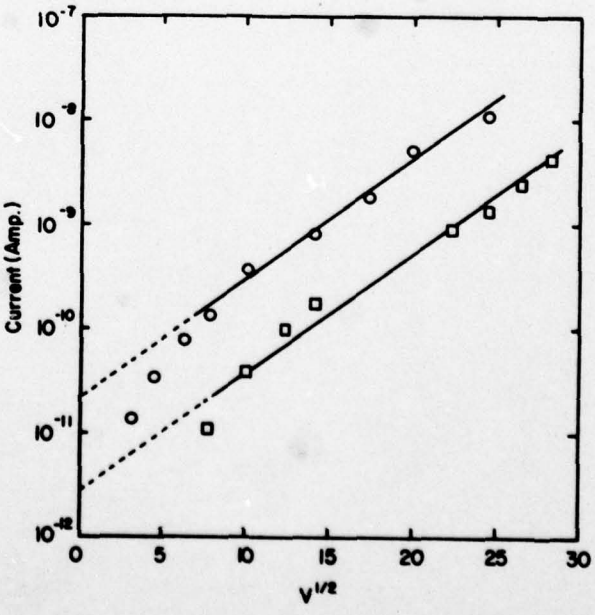

FIG. 6. Log current versus $V^{1/2}$ at 30 °C for a 6-μ-thick PVF_2 film with one Au and one Al electrode. ○: Au positively biased; □: Au negatively biased.

hydrogen bonding works against poling induced dipole orientation. Further experiments are necessary to verify this conjecture.

ACKNOWLEDGMENTS

The authors acknowledge with thanks helpful and stimulating discussions with Dr. P. Love, Dr. L. F. Nichols, and Dr. C.S. Bak.

[1]H. Kawai, Jpn. J. Appl. Phys. 8, 975 (1969).
[2]E. Fukada and S. Takashita, Jpn. J. Appl. Phys. 8, 960 (1969).
[3]G. Pfister, M. Abkowitz, and R.G. Crystal, J. Appl. Phys. 44, 2064 (1973).
[4]J.H. McFee, J.G. Bergman, Jr., and G.R. Crane, Ferroelectrics 3, 305 (1972).
[5]P. Buchman, Ferroelectrics 5, 39 (1973).
[6]K. Nakamura and Y. Wada, J. Polym. Sci. A-2 9, 161 (1971).
[7]E.W. Aslaksen, J. Chem. Phys. 57, 2358 (1972).
[8]M.H. Litt, C. Hsu, and P. Basu, J. Appl. Phys. 48, 2208 (1977).
[9]N. Murayama and H. Hashizume, J. Polym. Sci. 14, 989 (1976).
[10]J.J. Crosnier, F. Micheron, G. Dreyfus, and J. Lewiner, J. Appl. Phys. 47, 4798 (1976).
[11]N. Murayama, J. Polym. Sci.-Polym. Phys. Ed. 13, 929 (1975).
[12]N. Murayama, T. Oikawa, T. Katto, and K. Nakamura, J. Polym. Sci.-Polym. Phys. Ed. 13, 1033 (1975).
[13]R.J. Shuford, A.F. Wilde, J.J. Ricca, and G.R. Thomas, Polym. Eng. Sci. 16, 1 (1976).
[14]H. Bukard and G. Pfister, J. Appl. Phys. 45, 3360 (1974).
[15]G. Lengyel, J. Appl. Phys. 37, 807 (1966).
[16]A.C. Lilly, Jr. and J.R. McDowell, J. Appl. Phys. 39, 141 (1968).
[17]W. Vollmann and H.-U. Poll, Thin Solid Films 26, 201 (1975).
[18]P.J. Reucroft and S.K. Ghosh, J. Non-Cryst. Solids 15, 399 (1974).
[19]A.I. Baise, H. Lee, B. Oh, R.E. Salomon, and M.M. Labes, Appl. Phys. Lett. 26, 428 (1975).
[20]H. Scher, D. Pai, and J. Mort, J. Appl. Phys. 44, 2908 (1973).
[21]R.E. Salomon, C.S. Bak, and M.M. Labes, J. Appl. Phys. 47, 1710 (1976).
[22]See W. Helfrich, *Physics and Chemistry of the Organic Solid State*, edited by D. Fox, M.M. Labes, and A. Weissberger (Interscience Publishers, New York, 1967), Vol. III.

ORGANIC COATINGS and PLASTICS CHEMISTRY

VOLUME 38

PREPRINTS OF PAPERS PRESENTED
AT THE 175th MEETING OF THE
AMERICAN CHEMICAL SOCIETY

DIVISION OF
ORGANIC COATINGS
AND
PLASTICS CHEMISTRY

ANAHEIM, CALIFORNIA
MARCH 12-17, 1978

AMERICAN CHEMICAL SOCIETY

MECHANISTIC STUDIES OF PYROELECTRICITY IN POLY(VINYLIDENE FLUORIDE) AND BLENDS WITH OTHER POLYMERS

by

K. Takahashi, H. Lee, R. E. Salomon and M. M. Labes

Department of Chemistry, Temple University, Philadelphia, PA 19122

Pyro- and piezoelectricity in poly(vinylidene fluoride) (PVF_2) are thought to be due to the existence of an oriented dipolar structure induced by "poling" polymer films in a high dc field ("dipole-reorientation" model), or to the existence of a non-homogeneous space charge distribution ("space-charge" model), or both phenomena superimposed. The purpose of this study was to vary the crystallinity and phases of PVF_2 by blending it with poly(vinyl fluoride) (PVF) and poly(methyl methacrylate) (PMMA), and attempt to correlate pyroelectric behavior with the extent of crystalline phase present. If such a correlation exists, it would be hard to rationalize it in terms of a space-charge model, i.e. further credence would be added to the dipole-reorientation model.

Morphological studies have shown that there are three crystalline forms of PVF_2. The α-form (form II) has the trans-gauche-trans-gauche' configuration and the β-form (form I) has the planar zig-zag conformation. The structure of the γ-form (form III) is not established. However, there are some reports claiming that the γ-form is very similar to the β-form. The $-CF_2-$ group of the monomer unit has a dipole moment of 2.1 D. The β-form contains two parallel chains and two monomer units per unit cell with a net polarization of 1.3×10^5 Ccm^{-2}. The α-form contains two antiparallel chains and four monomer units per unit cell. The average dipole moment per monomer unit in the individual α-chains is approximately half of that in the β-chains, but the net polarization in the α-phase is zero due to the antiparallelism of the chains. Polymer blends of PVF_2 with poly(vinyl fluoride) (PVF) and poly(methyl methacrylate) (PMMA) were cast as films from N,N-dimethylformamide solution; the films were electroded with vacuum evaporated Nichrome, and the samples were poled at 10^6 Vcm^{-1} at 80° for 30 minutes. % crystallinity and extent of α, β, γ and amorphous phases were evaluated by both x-ray diffraction and infrared spectroscopy.

PVF_2/PMMA and PVF_2/PVF blends show strikingly different behaviors (Fig. 1). In the former, pyroelectric activity decreases monotonically as PMMA content increases and vanishes at 50% PMMA. In the latter, pyroelectric activity reaches a maximum at 11.5% PVF. Determinations of the % crystallinities and phases show that the pyroelectric coefficients are clearly correlated with the extent of β + γ phases in both of these blend systems (Fig. 2). These observations are consistent with a dipole reorientation model for pyroelectricity. It would be highly fortuitous if the extent of trapped charge and its distribution correlated with crystallinity in blends of PVF_2 with both PVF and PMMA.

Three possible mechanisms are considered for the dipole-reorientation process: (1) rotation of the individual chain around its own chain axis; (2) rotation of the polar domains; and (3) a combination of (1) and (2). NMR, dielectric and mechanical relaxation studies have shown that restricted rotations are allowed in the crystalline phases as well as in the amorphous phases. Furthermore, the onset of rotational motion in the α-phase occurs at a lower temperature (∿ 70°C at 110 Hz) than in the β-phase (∿ 110°C at 110 Hz). In the amorphous phase, motion occurs at an even lower temperature. If the individual chains could rotate around their own chain axes and retain this orientation, then they should exhibit some pyroelectricity. It would be reasonable to assume that the easier it is to rotate the chains, the faster the depolarization

process would be. Therefore, we suggest that the amorphous and α-phases are not able to retain enough polarization to give any observable pyroelectric current in the second heating cycle.

With respect to the poling process and trapped charge in poled PVF_2, analyses were undertaken of the steady state current-time-voltage-temperature relationships. Steady state currents at high fields and temperatures were found to follow the Richardson-Schottky (RS) equation closely (see Figs. 3 and 4). At lower fields and temperatures, however, the observed data are consistent with either a RS or space-charge-limited current analysis. In studies with layered films of PVF_2 with Mylar, it was clear that the largest pyroelectricity is observed when PVF_2 is in contact with the positively biased metal electrode, and in studies with different metal electrodes, it was also established that hole injection is the dominant process in the poling process.

Attempts were made to observe pyroelectricity arising from inhomogeneous space charge distribution, which has been estimated to be many orders of magnitude smaller than that observed in PVF_2 poled under normal conditions. Indeed when PVF_2 is poled at low fields at room temperature, or when a poly(20% acrylonitrile-80% vinylidene-chloride) is poled, a pyroelectric coefficient is observed which is consistent with the earlier published theoretical estimates by this group.

The support of ARO(D) under Grant No. DAAG29-76-G-0040 is gratefully acknowledged.

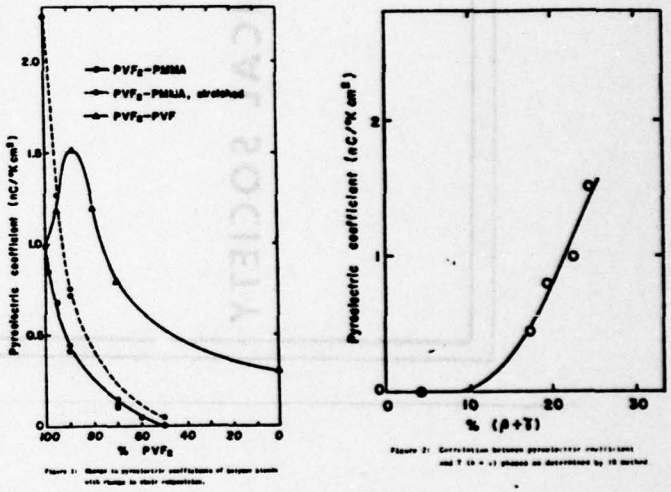

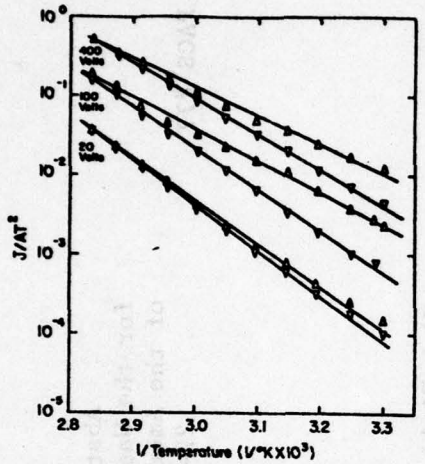

Figure 3: Log J/AT^2 vs $1/T$ at several voltages for a 6μ thick PVF_2 film with nichrome electrodes. △ increasing temperature; ▽ decreasing temperature during measurement. ⊠ equation: $J = AT^2 \exp(-\phi_0/kT)\exp(\beta_0 V^{\frac{1}{2}})$

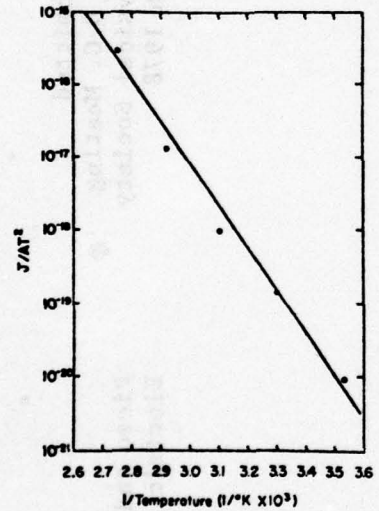

Figure 4: Log J/AT^2 plotted as a function of $1/T$. The slope gives the Schottky barrier, ~1 eV.

Influence of Metal Electrodes on the Polarization of Poly(vinylidene fluoride)

by
H. Sussner and D. Y. Yoon

IBM Research Laboratory
San Jose, California 95193

INTRODUCTION

Using a variety of experimental techniques it is now well established that the polarization of poly(vinylidene fluoride) (PVF_2) resultant from usual poling conditions is not uniform but rather strongest near the positive metal electrode during poling [1,2]. Furthermore, blocking the positively charged electrode, i.e., inserting a layer of insulating material between the polymer and the metal electrode, resulted in a drastic reduction of the polarization [2,3], whereas a blocking contact at the negative electrode hardly affected the induced polarization at all. Although these experiments clearly demonstrate the importance of the polymer-metal interface, several key questions about the nature of these interfacial processes still remain unanswered. In this regard it seems particularly important to manifest the influence of metal electrodes without changing the usual metal/polymer/metal conducting contacts, since the actual voltage drop across the polymer is no longer disputable as it is with the blocking electrodes [4].

Therefore, we have investigated the influence of the work function ϕ_M of the contacting metal electrodes on the induced polarization of PVF_2. Metal/polymer/metal sandwiches were prepared using combinations of Pt(ϕ_M=5.3 eV) with Mg(ϕ_M=3.6 eV) and Au(ϕ_M=4.8 eV) with Al(ϕ_M=4.2 eV) [5]. They were poled with different polarities, i.e., Pt(+)/Mg(-) vs. Pt(-)/Mg(+), under conventional conditions. Here we present the experimental results of the current-voltage characteristics, and the pyroelectric activities for these PVF_2 films under various combinations of poling conditions.

EXPERIMENTAL PROCEDURES

All of our experiments reported here were carried out using PVF_2 films of 12μ in thickness obtained from Kureha Chem. Corp. Circular electrodes of ~1000Å in thickness were deposited under high vacuum, 10^{-7} Torr, to cover an area of ~0.2 cm^2. Three different sets of metal/polymer/metal sandwiches were prepared; Pt/PVF_2/Mg, Au/PVF_2/Al, and Al/PVF_2/Al. In order to prevent the oxidation of Mg electrode when exposed to air, a 500Å thick Mg layer was subsequently overcoated with a 500Å thick Pt layer inside the vacuum chamber.

The current-voltage characteristics were measured at the poling temperature before and after poling in order to follow the space charge characteristics within the sample. The voltage was increased stepwise at the interval of 30 sec, and the current was measured at 30 sec after each voltage increase.

The pyroelectric coefficients of poled samples were measured using the dielectric heating method, which is described in detail elsewhere [6]. The uniformity of polarization was determined from the transient pyroelectric response [1].

RESULTS

The current-voltage (I/V) characteristics at 103°C for PVF_2 films with Pt/Mg and Al/Al electrode configurations are shown in Figure 1. We find

Abstract Submitted
for the Washington D.C. Meeting
of the American Physical Society

PACS #77

27-30 March 1978

Piezo and Pyro-Electric Effects

High Field Poling of Polyvinylidene Fluoride Film From -196° to +80°C.* K. TAKAHASHI, R. E. SALOMON AND M. M. LABES, Temple U.--The use of high strength dielectric media such as liquid "Fluorinert", SF_6 vapor, or high vacuum allows the application of dc fields up to 4.2×10^6 Vcm^{-1} to polyvinylidene fluoride (PVF_2) films at a wide variety of temperatures. Poling for 1 minute at room temperature or above is sufficient to cause saturation of the pyroelectric activity. In biaxially stretched (Kureha) 6μ film, a maximum pyroelectric coefficient of 4.2 $nCcm^{-2}\ {}^{o}K^{-1}$ (measured at 40°C) can be achieved by poling at 3×10^6 Vcm^{-1} at 80°C. Even at liquid nitrogen temperature, pyroelectric activity is induced by high field poling.

*Supported by ARO(D) Grant No. DAAG29-76-G-0040

Prefer Standard Session

M. M. Labes
Department of Chemistry
Temple University
Philadelphia, PA 19122

Frequency Dependence of Pyroelectric Current in Poly(vinylidene fluoride) Heat Sinked at Various Temperatures

L. F. Hu, K. Takahashi, R. E. Salomon and M. M. Labes*

Department of Chemistry, Temple University, Philadelphia, Pennsylvania 19122

Abstract

The frequency and temperature dependences of pyroelectric activity in poly(vinylidene fluoride) have been studied from 10°K to 369°K using mechanically chopped and steady state radiation. From these data, thermal diffusivity and a parameter indicating the polarization inhomogeneity can be deduced and compared with a mathematical model.

INTRODUCTION

In the utilization of poly(vinylidene fluoride), PVF_2, as an optical-radiation detector, the frequency response characteristics have been mathematically modeled by considering the interaction of two factors: (a) the inhomogeneity (or homogeneity) of the sample polarization as a consequence of the poling conditions, and (b) the thermal diffusivity of the pyroelectric material.[1-4] In this work, the frequency response to a pulsed heat input of a heat sinked PVF_2 film is examined. The temperature of the heat sink is varied from $369^{o}K$ to $10^{o}K$. Pyroelectric coefficients and thermal diffusivity are determined for PVF_2 in this temperature range. These experiments allow one to measure thermal diffusivity over a sufficient temperature range to check the validity of the mathematical model proposed by Peterson et al [1] to ascertain the inhomogeneity of polarization, and to determine the temperature dependence of the pyroelectric coefficient well above and below the glass transition temperature(s) of this semicrystalline polymer.

THEORY

A general description and solution for various boundary conditions of a pyroelectric detector have been described elsewhere in detail.[1] In this paper, the specific case considered is one in which one side of a PVF_2 film is kept at a fixed temperature with a heat sink, while the other surface is exposed to a chopped optical beam. Assuming that the input heat of the chopped optical beam is absorbed on the front surface without any loss, and heat flow is only in the x direction normal to the surface, one can express the current density resulting from changing the temperature of the pyro-

electric film as[1]

$$J(t) = 1/L\int_0^L dx \frac{dP}{dT}\frac{dT(x,t)}{dt} \qquad (1)$$

where L is the thickness of the pyroelectric film, T is the temperature, t is the time and dP/dT is the pyroelectric coefficient. For convenience, the functional relationship to express the nonuniformity of the pyroelectric coefficient throughout the film used in this calculation is

$$dP/dT = P_0 \exp(-\xi x/L) \qquad (2)$$

where P_0 is the surface pyroelectric coefficient and ξ is the parameter of nonuniformity.[1] One dimensional heat flow in the film gives

$$dT/dt = \alpha d^2T/dx^2 \qquad (3)$$

where α is the thermal diffusivity. The term α is defined as

$$\alpha = k/C_v \qquad (4)$$

where k is the thermal conductivity and C_v is the heat capacity per unit volume at constant pressure. Eq. (3) is solved using the following boundary conditions: a perfect heat sink keeps one end of the film at a constant temperature,

$$T(x = L,t) = T_0 \; ; \qquad (5)$$

heat is supplied in some specified manner to the exposed face at x = 0, expressed by the equation

$$Q = -k\, dT/dx \qquad (6)$$

where Q is the heat input. The steady-state current response to a sinu-

soidal heat input at frequency w_0 is given in Ref. (1) as

$$|J(w_0)| = (P_0 Q_0 / LC_v)|\bar{\gamma}(iw_0)| \tag{7}$$

where Q_0 is the incident heat. The complex response function $\bar{\gamma}(iw)$ to the heat input is

$$\bar{\gamma}(iw) = \frac{\mu(e^{-2W_p}-1) + (1 + e^{-2W_p}) - 2e^{-\xi-W_p}}{(1 + e^{-2W_p})(1 - \mu^2)} \tag{8}$$

where $W_p = (iw/\alpha)^{\frac{1}{2}}L$ and $\mu = \xi/W_p$. The magnitude of the current density $|J(W_0)|$ in Eq. (7) is obtained by calculating $(\bar{\gamma}(iW_0)\bar{\gamma}^*(iW_0))^{\frac{1}{2}}$.

EXPERIMENTAL

Both sides of biaxially stretched 6 μ PVF_2 films, obtained from Kureha Chemical Corporation, were vacuum deposited with nichrome electrodes. The thickness and area of the electrodes were 150 Å and 1.3 cm^2, respectively. Electrical leads were attached with conducting epoxy adhesive (Acme Chemical, No. 3021). The samples were poled at 60°C with fields of 1,2 or 3 $MVcm^{-1}$. For the first heating cycle, the poled films were heated at 10°C min^{-1} from the poling temperature of 60°C up to 80°C and kept at 80°C for 10 minutes in the short circuit configuration. The samples were then cooled to room temperature. During a second heating cycle, the samples were heated at 2°C min^{-1} and pyroelectric currents were measured. Pyroelectric coefficients were calculated at a temperature of 35°C. A detailed description of this measurement and the subsequent calculation of the pyroelectric coefficient are reported elsewhere.[5] For poling of films at fields of more than 2 $MVcm^{-1}$, a dielectric liquid (Fluorinert FC-77) was used. During

poling, the films were dipped in the liquid to prevent short circuits in the film.

The poled films were mounted on two different heat sinks, one for the experiments at room temperature, and the other for experiments at various temperatures ranging from 10^{o}K to 369^{o}K. For the experiments at room temperature, Cry-Con Grease (Air Products and Chemicals) or General Electric No. 7031 adhesive insulating varnish was used to attach the sample to a copper plate heat sink. The copper plate was mounted in an aluminum box for shielding to prevent extraneous noise. For experiments at various temperatures, the films were glued to the plane of a copper column, which was used as a heat sink, with General Electric No. 7031. The copper column was mounted in a Displex Cryostat (Air Products and Chemicals, Model CSA-202). A chromel-alumel thermocouple was placed in a hole in the copper column with Cry-Con Grease so that the heat sink temperature could be read out with a millivolt potentiometer or Keithley 160 Digital Multimeter. For both cases, the back nichrome electrode was grounded to the heat sink. The upper nichrome electrode was connected to a lock-in amplifier (PAR Model 124). A load resistor of 47 KΩ was inserted in parallel with the sample. A tungsten lamp was used as the heat source. The light beam was chopped with a PAR Model 222 chopper to form a square wave. The signal response was measured from a low frequency of 10 Hz to a high frequency of 4500 Hz.

Experiments with the heat sink at various temperatures were carried out in a vacuum since this is a requirement for use of a Displex Cryostat. At 290^{o}K experiments were conducted in both vacuum and air.

Since the results were essentially the same, the thermal conductivity of air could be neglected. To determine the effect of the thickness variation of the heat absorbing nichrome electrode, a sample in which the electrode thickness of the exposed side was half of that of the typical thickness (150 Å) was prepared. The results in terms of the chopper frequency, the magnitude of the maximum pyroelectric current, and the overall shape of the curve were the same indicating a negligible effect of the absorber thickness, at least in these experimental ranges of heat sink temperature and chopper frequency.

To check linearity of response (which will be crucial to the subsequent analysis), the incident light was varied by placing screens between the light and the sample and was measured with a thermopile. It was found that the pyroelectric response varied linearily with the incident light of the frequency range used in this experiment.

RESULTS AND DISCUSSION

Typical curves of the pyroelectric current vs. the chopper frequency are shown in Fig. 1. The chopper frequency at the maximum pyroelectric current in the curve shifted with the heat sink temperature. At the lower temperature, the maximum current appeared at the higher frequency. Pairs of samples were examined for a comparison between the cases for radiation absorbed on the positively and negatively poled side. At any temperature of the heat sink, the positively poled side always had a larger pyroelectric current than the corresponding negatively poled side, as shown in Table I.

The results in Table II show that the distribution of polarization

through the film is not uniform. It is generally assumed that dP/dT varies with x as $P_0 \exp(-\xi x/L)$, where x is the distance through the film from the irradiating electrode, L is the thickness of the film, and P_0 is the surface pyroelectric coefficient.[1] When the measurement is made with the negatively poled side exposed to the chopped radiation, dP/dT can be expressed as $P_0 \exp(-\xi)\exp(\xi x/L)$. From the results, it is obvious that the value of ξ should be positive. The theoretical and experimental curves were superimposed enabling us to find a value for ξ by matching magnitudes of the maximum pyroelectric currents and frequencies.

These ξ values determined for samples measured at low temperatures and at room temperature are listed in Table II. It is apparent that the larger ξ is due to a greater nonuniformity of the polarization. When the poling field is smaller, a greater inhomogeneity of polarization is produced through the film. These results are basically in agreement with the literature results.[4]

According to the theoretical model,[1] W_p is a function of the thermal diffusivity α. Thus, the quantity W_p is temperature dependent and causes the frequency of the maximum pyroelectric current to vary with temperature. To verify this, it is necessary to determine whether the shape of the frequency dependent pyroelectric current and hence the ξ value was affected by changing the temperature. Data obtained at three different temperatures were replotted as shown in Fig. 2. It is apparent that the overall shape of the curves are not affected by varying the temperature, although the original frequency dependent curves have different frequencies and magnitudes at the maximum pyroelectric current. Also, the values of ξ

at low temperatures were not significantly changed as listed in Table II. Therefore, the value of ξ or the distribution of polarization is temperature independent and the shift of the frequency at the peak pyroelectric current is caused by the change of α at different temperature, that is, the value of the thermal diffusivity (k/C_v).

Using available data for thermal diffusivity,[6] theoretical response curves were plotted at different temperatures as shown in Fig. 3. In each curve a single peak appears at a certain frequency below 10^4 Hz and the shift of the frequency at the peak is observed at different temperatures. The peak arising for the case of irradiation on the positively poled side appeared at a slightly higher frequency than the one for the reverse case even at low temperatures. This characteristic was observed for all the experimental results shown in Table III.

Experimental values of thermal diffusivity at different temperatures were calculated from the peak frequencies. Using these thermal diffusivity data and available heat capacity data,[7] the thermal conductivities at different temperatures were calculated. These results are listed in Table III and thermal conductivities vs. temperatures are plotted in Fig. 4. Some slight differences exist between the results obtained and the available literature values. The peak frequency in the theoretical curve is at 600 Hz at room temperature, and does not match precisely with the peak observed experimentally (1000 Hz). These discrepancies are probably due to such differences as molecular weight distribution in the polymer samples and the differences in the methods of preparation, one set of data being taken on film pressed from a powder and the other on a biaxially stretched film.

The thermal conductivity of the film can be treated by a two phase

model in which the conductivity of the amorphous regions is essentially isotropic while that of the crystalline regions is highly anisotropic. The thermal conductivities obtained here are for the direction perpendicular to the crystals with the chain axes parallel to the stretching direction. At temperatures of more than 100°K, a leveling off of the thermal conductivity was observed. This is probably due to the conductivity via the weak Van der Waals interactions perpendicular to the chains, which is undoubtedly much smaller than through the strong covalent bonds along the chains. Thus crystallites aligned parallel to the stretching direction contribute more to the thermal conductivity. At temperatures lower than 100°K, a sharp decrease of the conductivity was observed. As the phonon wavelength becomes greater than the size of the crystallites at these temperatures, the acoustic mismatch at the crystalline or crystalline-amorphous boundaries may give rise to a sharp increase in thermal resistance.

The pyroelectric current J is given by $\frac{P_o Q_o}{L C_v}|\gamma|$. The quantity of heat Q_o and the thickness L are constant. The magnitude of the pyroelectric current J is a function of P_o and C_v which are temperature dependent parameters. Using literature data for C_v,[7] the relative pyroelectric coefficients of a given film at different temperatures can be calculated by taking a ratio. The results are shown in Fig. 5. It can be seen that the relative pyroelectric coefficient increases with increasing temperature. The nature of the temperature dependence changes at $\sim$ 220°K. Below this temperature, the pyroelectric coefficients are moderately temperature dependent but above this temperature they exhibit a T^2 dependence. The temperature of 220°K is close to the glass transition temperature of PVF_2.[8] Probably below the temperature of 220°K the material becomes stiff with no

expansion of volume and the primary coefficient is the main contribution, while above this temperature, the thermal expansion of the film becomes large and the secondary coefficient contributes significantly. The pyroelectric coefficients in the temperature range between 253°K to 373°K are found to exhibit a T^3 dependence using the conventional method of pyroelectric measurements.[9] The reason for the different temperature dependences of the pyroelectric coefficients in this temperature range may be related to the temperature dependences both of the heat capacity and thermal conductivity. A dilatometric study shows an $\sim T^2$ dependence of thermal expansion of PVF_2 in the temperature range between 243°K to 373°K,[10] offering additional evidence that pyroelectric coefficients in this temperature range are associated with thermal expansion.

CONCLUSIONS

Pyroelectric coefficients for PVF_2 have been measured from 10°K to 369°K. The pyroelectric coefficients are moderately temperature dependent from 10°K to the glass transition temperature and exhibit a T^2 dependence from the glass transition temperature to 369°K.

The inhomogeneity introduced by poling is shown to be temperature independent. This strongly suggests that the origin of pyroelectricity in PVF_2 cannot be based on an equilibrium thermodynamic model, such as the Devonshire model of ferroelectrics.[11]

Thermal diffusivity deduced from data on pyroelectric current produced by pulsed heating from 20°K to 290°K is consistent with data in the literature. Even over this extended temperature range, the mathematical model of Peterson et al,[1] based on considering only the temperature dependence

of the thermal diffusivity and the extent of polarization inhomogeneity is adequate to explain the results.

REFERENCES

*This work was supported by the U. S. Army Research Office under Grant No. DAAG29-76-G-0040.

1. R. L. Peterson, G. W. Day, P. M. Gruzensky and R. J. Phelan, Jr., J. Appl. Phys. 45, 3296 (1974).
2. R. J. Phelan, Jr. and A. R. Cook, Appl. Opt. 12, 2494 (1973).
3. G. W. Day, C. A. Hamilton, R. L. Peterson, R. J. Phelan, Jr. and L. O. Mullen, Appl. Phys. Lett. 24, 456 (1974).
4. G. W. Day, C. A. Hamilton, P. M. Gruzensky and R. J. Phelan, Jr., Ferroelectrics 10, 99 (1976).
5. A. I. Baise, H. Lee, B. Oh, R. E. Salomon and M. M. Labes, Appl. Phys. Lett. 26, 428 (1975).
6. F. C. Chen, Y. M. Poon and C. L. Choy, Polymer 18, 129 (1977).
7. W. K. Lee and C. L. Choy, J. Polym. Sci., Part A-2, 13, 619 (1975).
8. G. Pfister and M. A. Abkowitz, J. Appl. Phys. 45, 1001 (1974).
9. K. Takahashi, R. E. Salomon and M. M. Labes, unpublished results.
10. J. B. Enns and R. Simka, J. Macromol. Sci., B, 13, 11 (1977).
11. E. Fatuzzo and W. J. Merz, in Ferroelectricity (North Holland Publishing Company, Amsterdam, 1967), p. 105.

Table I. Maximum Pyroelectric Currents Under Various Poling Conditions as a Function of Temperature

Sample[a]	Poling Conditions[b] E_p(MV cm^{-1})	t_p(min)	Pyroelectric Coefficient at 308°K[c] ($nCcm^{-2}K^{-1}$)	Pyroelectric Response (μV) 20°K	50°K	100°K	150°K	200°K	233°K	250°K	290°K[d]
20+	1	60	0.92	5.2	5.6	5.1	4.9	4.1	--	4.5	5.3
20-	1	60	1.10	2.9	2.8	2.3	1.9	1.8	1.8	1.9	2.2
21+	1	60	1.37	5.3	4.2	4.1	4.6	4.6	4.8	5.0	6.1
21-	1	60	1.48	4.0	4.3	4.0	3.6	3.4	3.4	3.6	4.3
25+	2	30	2.80	4.4	4.5	3.9	3.5	3.2	3.2	3.4	4.0
25-	2	30	2.60	2.9	3.0	2.7	2.6	2.5	2.3	2.5	3.1
26+	2	30	2.60	6.5	6.6	6.2	5.5	5.2	5.4	--	6.9
26-	2	30	2.77	5.4	5.5	5.0	4.5	4.1	4.0	4.0	4.6
75+	1	60	1.15	4.8	5.1	4.6	4.2	3.9	4.0	4.2	5.1
1+	1	30	--	--	--	--	--	--	--	--	26
1-	1	30	--	--	--	--	--	--	--	--	12
2+	1	60	1.26	--	--	--	--	--	--	--	24
2-	1	60	1.30	--	--	--	--	--	--	--	17
3+	2	30	2.56	--	--	--	--	--	--	--	20
3-	2	10	2.65	--	--	--	--	--	--	--	13

Table I (cont'd.)

Sample[a]	Poling Conditions[b] E_p (MV cm^{-1})	t_p (min)	Pyroelectric Coefficient at 308°K[c] ($nCcm^{-2}K^{-1}$)	Pyroelectric Response (μV) 20°K	50°K	100°K	150°K	200°K	233°K	250°K	290°K[d]
4+	3	5	2.96	--	--	--	--	--	--	--	26
4-	3	5	2.82	--	--	--	--	--	--	--	25

(a) The samples designated by the same number indicate pairs which were prepared identically. The notation + and - indicates irradiation on the positively poled side or negatively poled side, respectively.

(b) E_p and t_p are poling field and time, respectively.

(c) Measured by the conventional method.

(d) The incident light intensity used in irradiating samples 1-4 was much larger than all other samples, and hence the absolute currents are also larger.

Table II. Nonuniformity Parameter ξ for Various Samples as a Function of Temperature

Sample	Values of ξ at Various Temperatures							
	20°K	50°K	100°K	150°K	200°K	233°K	250°K	290°K
20	0.6	0.7	0.8	1.0	0.9	--	0.9	0.9
21	0.3	0.0	0.0	0.3	0.3	0.3	0.3	0.3
25	0.4	0.4	0.4	0.3	0.3	0.3	0.3	0.3
26	0.2	0.2	0.2	0.2	0.3	0.3	--	0.4
1	--	--	--	--	--	--	--	0.8
2	--	--	--	--	--	--	--	0.3
3	--	--	--	--	--	--	--	0.4
4	--	--	--	--	--	--	--	0.0

Table III. Temperature Dependence of Frequency (Hz) at Which Maximum Pyroelectric Current is Observed

Sample[a]	Peak Frequency (Hz)							
	20°K	50°K	100°K	150°K	200°K	233°K	250°K	290°K
20+	3000	2600	2300	2000	1700	--	1000	900
20-	3300	2900	2200	1900	1600	1300	1100	1000
21+	3400	3000	2600	2250	1800	1400	1200	1000
21-	3200	2700	2300	1800	1500	1300	1000	900
25+	3500	3100	2300	2000	1700	1300	1300	1000
25-	3700	3000	2400	1850	1700	1450	1150	1000
26+	3700	3000	2500	1750	1600	1250	--	1050
26-	3000	2700	2200	1900	1500	1200	1050	800
75+	3600	3000	2500	2100	1900	1500	1200	1050
Average								
+	3440	2940	2440	2020	1680	1360	1180	1000
-	3300	2830	2280	1860	1580	1310	1080	930

(a) The sample notation is the same as described in Table I.

Table IV. Comparison of Calculated Thermal Conductivity and Diffusivity with Literature Values

Temperature	Thermal Conductivity		Diffusivity	
^{o}K	Calculated ($W\ m^{-1}\ ^{o}K^{-1}$)	Literature[7] ($W\ m^{-1}\ ^{o}K^{-1}$)	Calculated $x10^{7}(m^{2}sec^{-1})$	Literature[7] $x10^{7}(m^{2}\ sec^{-1})$
290	0.200[a]	0.200	0.92[a]	0.92
250	0.199	0.196	1.07	1.08
233	0.204	0.193	1.21	1.13
200	0.222	0.187	1.58	1.29
150	0.205	0.172	1.86	1.54
100	0.178	--	2.25	--
50	0.113	--	2.75	--
20	0.038	--	3.21	--

(a) Calculated values were obtained by a comparison with this value which was taken from the literature.[7]

Figure Captions

Figure 1: Pyroelectric response vs log frequency at different temperatures for sample 21+.

▼ ,290°K; □ ,250°K; ○ ,150°K; △ ,50°K.

Figure 2: Relative pyroelectric response vs relative frequency at three different temperatures.

□ ,290°K △ ,150°K; ○ ,50°K.

Figure 3: Pyroelectric response vs log frequency using literature thermal diffusivity data.

(a) $\xi = 0$ (uniform polarization);

(b) $\xi = 0.6$, positively poled side irradiated;

(c) $\xi = 0.6$, negatively poled side irradiated.

The five curves from left to right are for temperatures of 290°K, 250°K, 233°K, 200°K and 150°K, respectively.

Figure 4: Log-log plot of thermal conductivity vs temperature.

Figure 5: Log-log plot of normalized pyroelectric coefficient vs temperature.

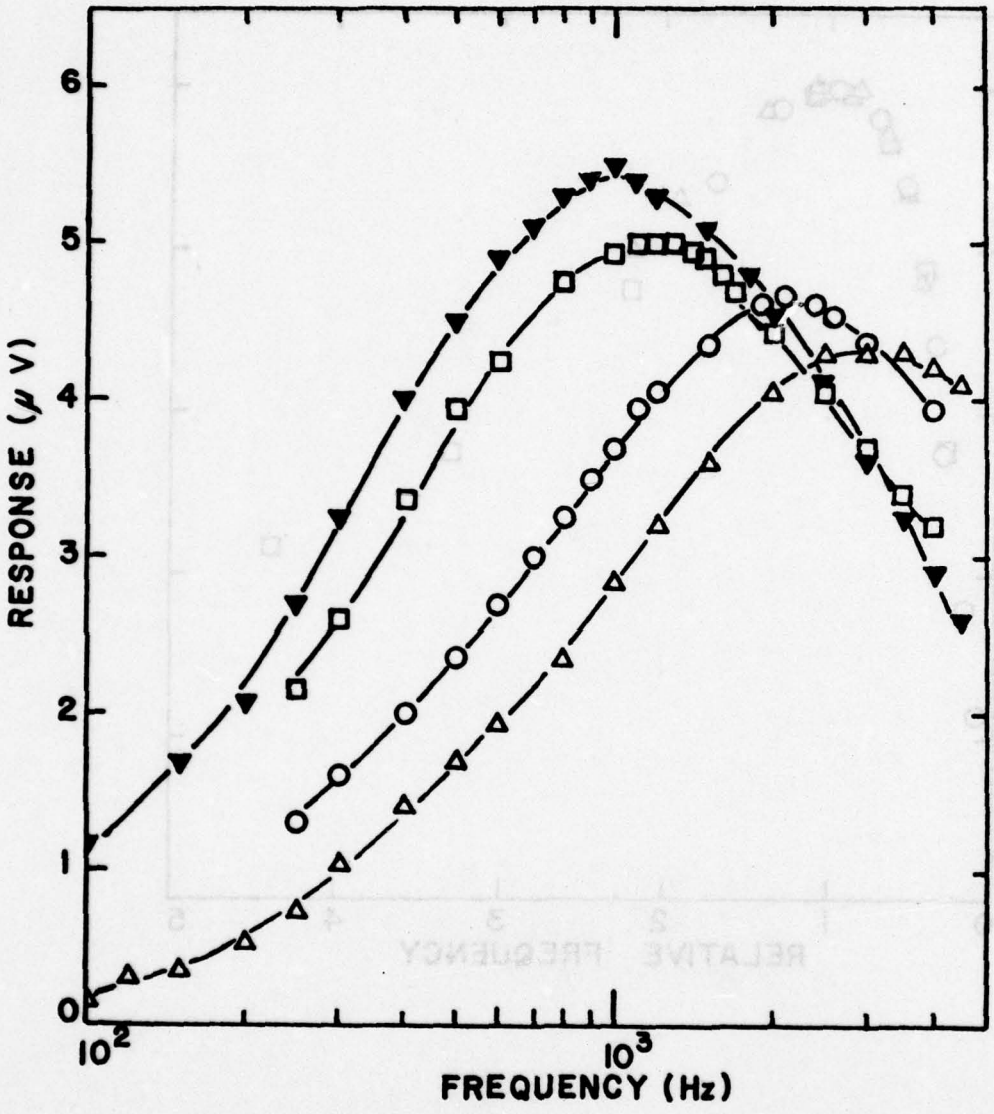
RESPONSE (μ V)
0
1
2
3
4
5
6
10^2
10^3
FREQUENCY (Hz)

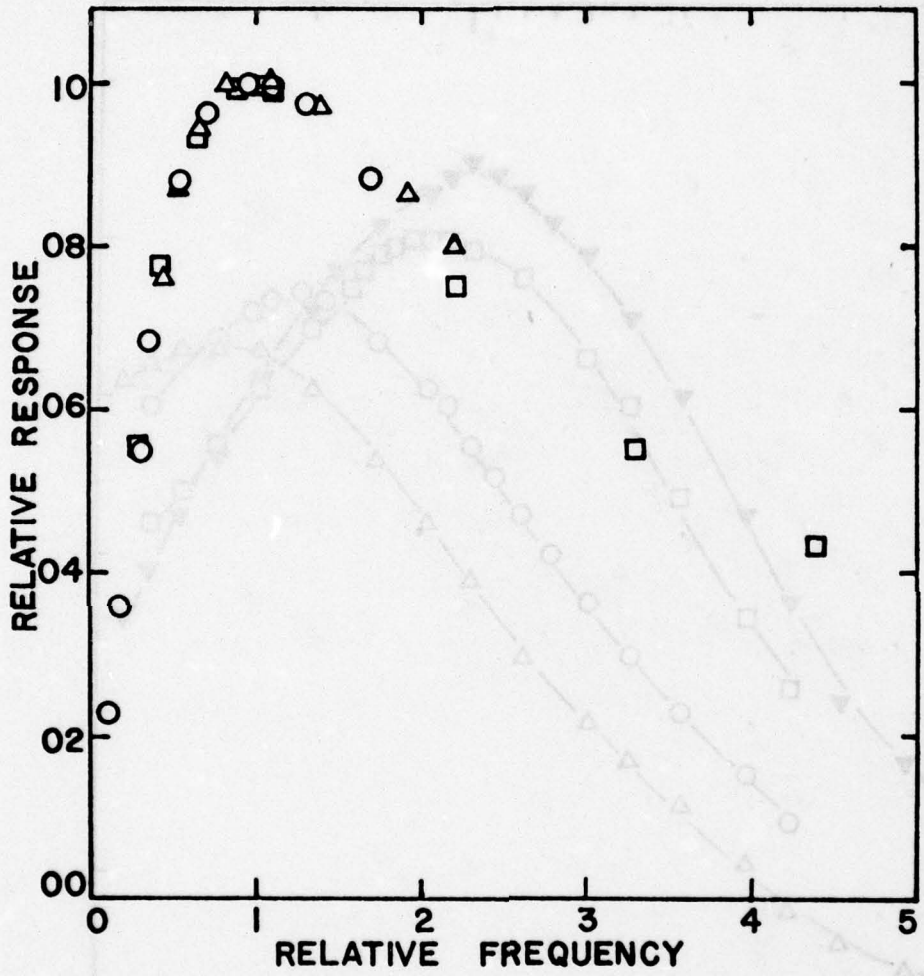
RELATIVE RESPONSE
10
08
06
04
02
00
0
1
2
3
4
5
RELATIVE FREQUENCY

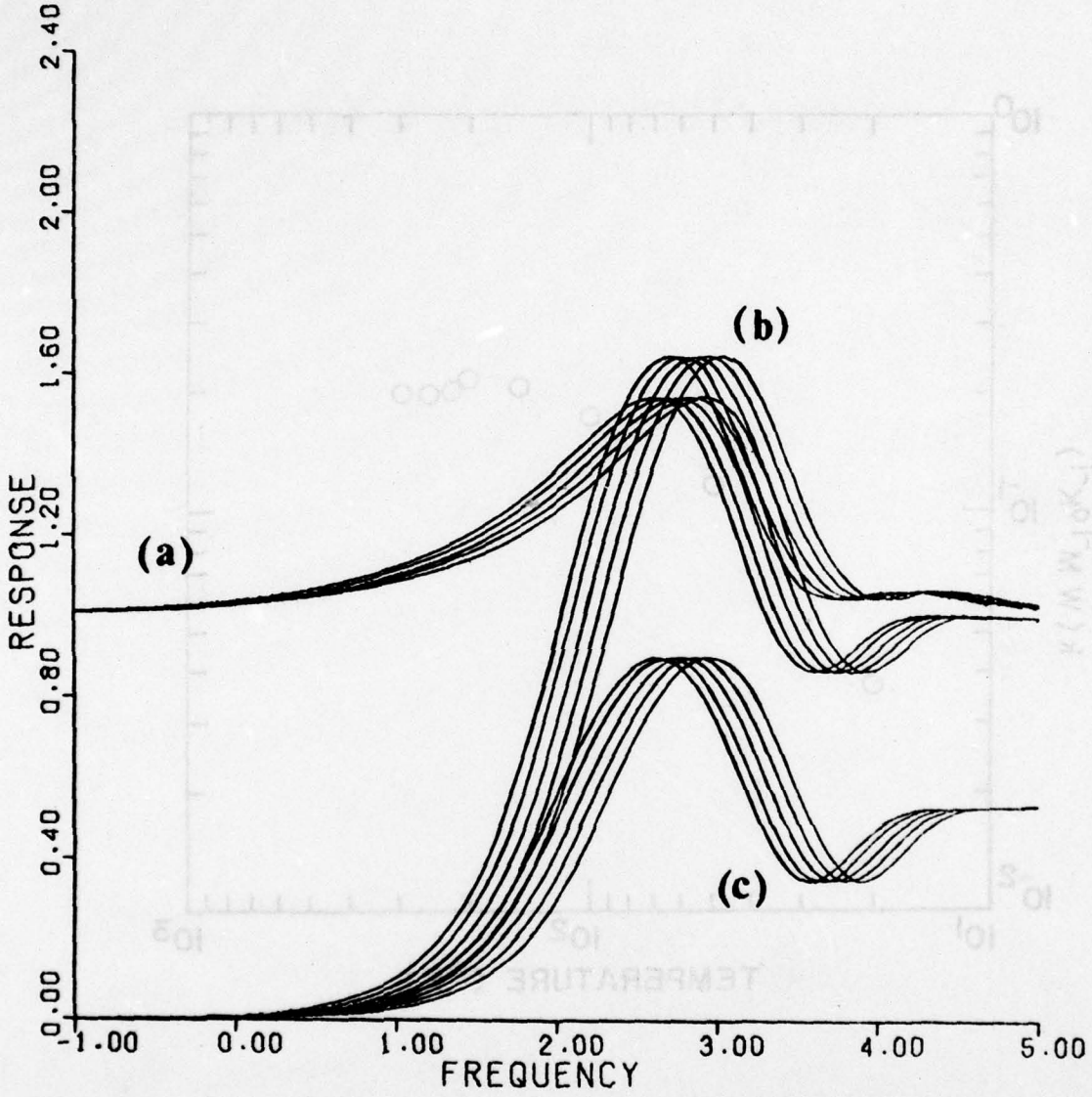
RESPONSE
0.00
0.40
0.80
1.20
1.60
2.00
2.40
(a)
(b)
(c)
-1.00
0.00
1.00
2.00
3.00
4.00
5.00
FREQUENCY

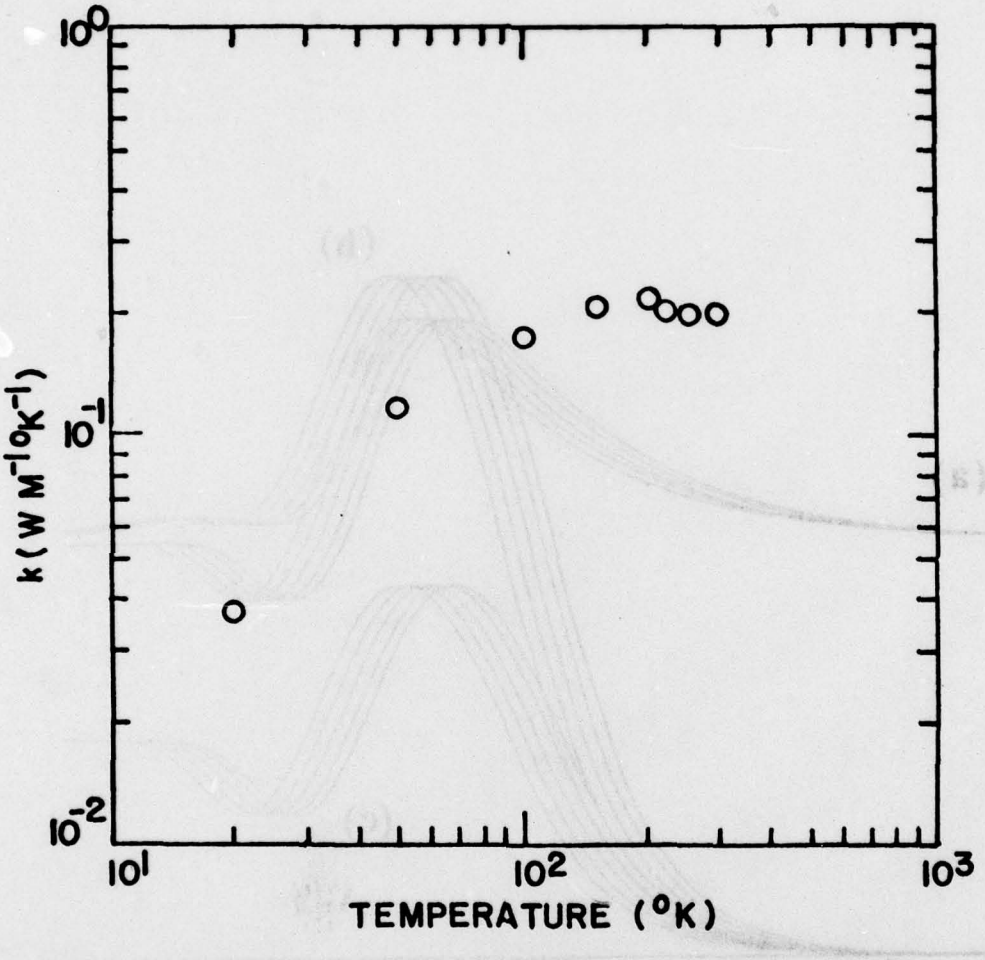
10^0
10^{-1}
10^{-2}
$k\,(W\,M^{-1}o K^{-1})$
10^1
10^2
10^3
TEMPERATURE (^oK)

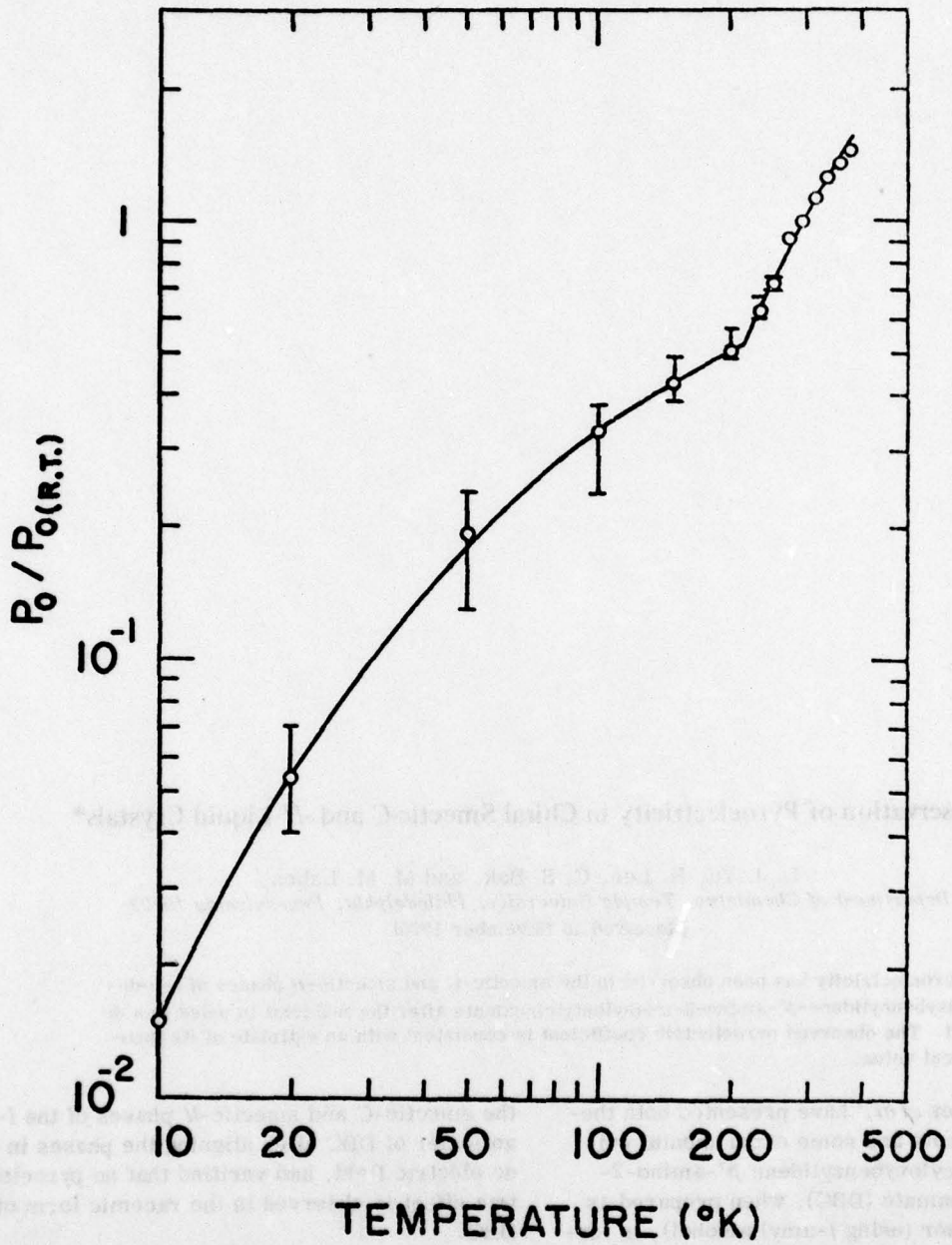
1
10^{-1}
10^{-2}
$P_0 / P_{0(R.T.)}$
10
20
50
100
200
500
TEMPERATURE (°K)

Observation of Pyroelectricity in Chiral Smectic-*C* and -*H* Liquid Crystals*

L. J. Yu, H. Lee, C. S. Bak, and M. M. Labes
Department of Chemistry, Temple University, Philadelphia, Pennsylvania 19122
(Received 10 November 1975)

Pyroelectricity has been observed in the smectic-*C* and smectic-*H* phases of *l*-*p*-decyloxybenzylidene-*p'*-amino-2-methylbutylcinnamate after the material is poled in a dc field. The observed pyroelectric coefficient is consistent with an estimate of its theoretical value.

Recently Meyer *et al.*[1] have presented both theoretical arguments and some experimental evidence that *p*-decyloxybenzylidene-*p'*-amino-2-methylbutylcinnamate (DBC), when prepared as a pure enantiomer (using *l*-amyl alcohol), is ferroelectric in the smectic-*C* and smectic-*H* phases. It occurred to us that an indication of spontaneous polarization in these phases would be the presence of a *pyroelectric* effect. We have succeeded in measuring a pyroelectric current in the smectic-*C* and smectic-*H* phases of the *l*-enantiomer of DBC after aligning the phases in a dc electric field, and verified that no pyroelectric effect is observed in the racemic form of DBC.

l- and *dl*-DBC were synthesized in the following manner[2]: *p*-nitrocinnamic acid was converted to the acid chloride via treatment with thionyl chloride; *l*-amyl alcohol or *dl*-amyl alcohol was then added to form the *p*-nitrocinnamate ester,

which was reduced to the *p*-aminocinnamate ester with stannous chloride and hydrochloric acid. Finally, the Schiff base DBC was made by condensing the *p*-aminocinnamate ester with *n*-decyloxybenzaldehyde. The phase transition temperatures were in good agreement with those previously reported.[1]

The pyroelectric measurements were performed on samples of *l*-DBC and *dl*-DBC aligned between two glass plates which had been coated with indium oxide and then with silicon monoxide to promote homogeneous alignment.[3] A 6.3-μm or 12.7-μm Mylar film with a 1.2×1.2-cm^2 hole was used as a spacer. The samples were heated to 125°C, 8° higher than the isotropic transition temperature, kept under a dc electric field of 5×10^4 V cm^{-1} for 1 h, and quenched to the smectic-*C* phase with the field still applied. This treatment serves two functions: Undesirable ionic species are removed by electrolysis, and the sample is "poled"; i.e., the dipoles are aligned in the field. Alternatively, the sample can be poled starting from the smectic-*A* phase (115–95°C). In the smectic-*C* and -*H* phases, the "spontaneous" currents are measured after the "background" current stabilizes, which takes ~2 h. A small residual background current is always observed; in *l*-DBC a pyroelectric current is also observed when the sample is heated (or cooled) at a rapid heating (or cooling) rate. The pyroelectric currents were measured in the smectic-*C* and -*H* (<63°C) phases. In the smectic-*A* phase, in accord with theory, no pyroelectric current could be observed. However, the background current in this phase was always quite high, and it would therefore be difficult to distinguish a pyroelectric current in this phase in any event.

In the experiments reported in this work, the molecular axis is parallel to the glass; i.e., the smectic planes are perpendicular to the glass and an electric field is applied perpendicular to the glass plates. A macroscopic dipole moment will only occur when the helicoidal smectic array is "untwisted," i.e., when the pitch approaches infinity. We found that after poling, the infinite-pitch smectic-*C* and -*H* phases were partially retained for several hours even after the field was removed; i.e., a memory state was achieved. Microscopic observations indicated that a large portion of the sample did not relax back to the so-called fingerprint texture; the helical array may be partially restored but with a large pitch.[4] For this reason, the structures of both the smectic-*C* and the smectic-*H* phases, being untwisted, should have a macroscopic dipole moment and should therefore show a pyroelectric effect. As a control experiment *dl*-DBC was treated in an identical manner; because of the apolar character of this material, no pyroelectric effect should be observable.

Pyroelectric currents were measured in a manner previously described.[5] The samples are first held at a fixed temperature until a stable background current is observed and recorded; heating rates of 75 and 10°/min for the smectic-*C* and smectic-*H* phases, respectively, were applied and the phases heated to a 5° higher temperature. As can be seen in Fig. 1, this heating produces a current pulse as well as a rise in the background current. The background current stabilizes again as soon as the temperature stabilizes. When no pyroelectric current is produced, as in the experiments with *dl*-DBC, one observes the rise in the background current, but no pyroelectric current pulse.

The pyroelectric coefficient dP/dT can be calculated from the data of Fig. 1 from the following expression for the pyroelectric current I:

$$I = A(dP/dT)dT/dt\,, \tag{1}$$

where A is the electrode area and dT/dt is the heating rate. The highest value of the pyroelectric coefficient in the smectic-*C* phase is $\sim 2\times10^{-11}$ C deg^{-1} cm^{-2}, and $\sim 3\times10^{-11}$ C deg^{-1} cm^{-2} in the smectic-*H* phase. The magnitude of the ob-

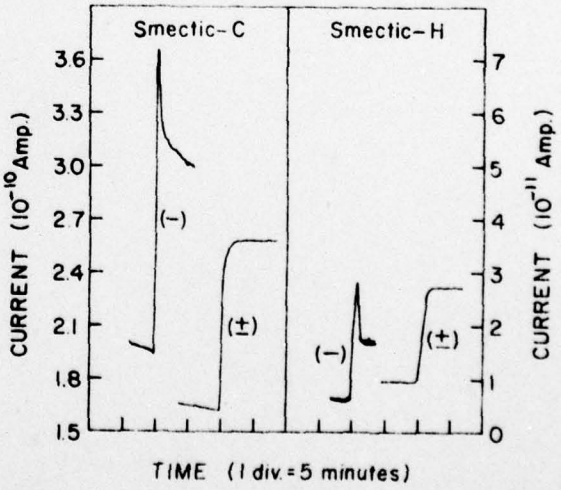

FIG. 1. Recorder tracings of observed currents in chiral (−) and racemic (±) DBC. The compounds are heated from 65 to 70°C at a rate of 75°/min in the smectic-C phase, and from 50 to 55°C at a rate of 10°/min in the smectic-*H* phase.

served pyroelectric coefficient was often as much as a factor of 2 less than this, the irreproducibility presumably related to the degree of alignment and memory state which exists in the individual sample.

An estimate of the theoretical value of dP/dT can be made in the following manner. Polarization P is defined as the macroscopic dipole moment per unit volume V:

$$P = N\bar{m}/V = \rho\bar{m}, \tag{2}$$

where N is the number of dipoles in the volume V, $\bar{m}$ is the dipole moment, and $\rho = N/V$. By differentiating Eq. (2) with respect to temperature T, one obtains

$$\frac{dP}{dT} = P\left(\frac{1}{\rho}\frac{d\rho}{dT} + \frac{1}{\bar{m}}\frac{d\bar{m}}{dT}\right). \tag{3}$$

The relative change in density $(1/\rho)d\rho/dT$ is approximately the volume expansion coefficient (negative sign) and should have the value of $\sim -1 \times 10^{-3}$ deg^{-1}.[6,7] The magnitude of the second term in Eq. (3) is -10^{-5} deg^{-1},[8] and can therefore be neglected.[9] P can be assumed[1] to have a value of ~ 125 esu cm^{-2} ($= 4.2\times 10^{-8}$ C cm^{-2}). Therefore an estimate of dP/dT is $\sim -4\times 10^{-11}$ C deg^{-1} cm^{-2}.

Thus the observed value of the pyroelectric coefficient [$(2$ to $3)\times 10^{-11}$ C deg^{-1} cm^{-2}] is quite close to the theoretical value. Since neither perfect alignment of smectic-C and -H phases nor perfect untwisting of the chiral phases can be assured, the agreement is rather good. Further work on describing the properties of these interesting phases is underway.

*This work was supported by the U. S. Army Research Office under Grants No. DAHC04-74-G-0186 and No. DAAG29-76-G-0040.

[1]R. B. Meyer, L. Liebert, L. Strzelecki, and P. Keller, J. Phys. (Paris), Lett. 36, L-69 (1975).

[2]M. Leclercq, J. Billard, and J. Jacques, Mol. Cryst. Liq. Cryst. 8, 367 (1969); A. Psarrea, C. Sandris, and G. Tsatsas, Bull. Soc. Chim. Fr. 1961, 2145.

[3]J. L. Janning, Appl. Phys. Lett. 21, 173 (1972).

[4]The lifetime of such a memory state seems to depend on the thickness and boundary conditions of the sample. Although Meyer *et al.* (Ref. 1) did not report memory effects in their earlier work, observations of long-lived untwisted states have also been made by them (R. B. Meyer, private communication).

[5]A. I. Baise, H. Lee, B. Oh, R. E. Salomon, and M. M. Labes, Appl. Phys. Lett. 26, 428 (1975).

[6]L. E. Hajdo, A. C. Eringen, A. E. Lord, Jr., and F. E. Wargocki, Lett. Appl. Eng. Sci. 3, 125 (1975).

[7]L. E. Hajdo, A. C. Eringen, J. Giancola, and A. E. Lord, Jr., Lett. Appl. Eng. Sci. 3, 61 (1975).

[8]R. G. Kepler, in "Proceedings of the Second International Conference on Electrophotography, October 1973" (Society of Photographic Scientists and Engineers, to be published).

[9]The polarization is expected to change rapidly near the smectic-C–smectic-A transition temperature [see, for example, R. Blinc, Phys. Status Solidi (b) 70, K29 (1975)]. Our measurements for the smectic-C phase were therefore carried out 20° below this transition point to avoid any contribution to the current from such a pretransitional phenomenon.

Pyroelectricity due to a Space-Charge Mechanism in a Copolymer of Acrylonitrile and Vinylidene Chloride

H. Lee, R. E. Salomon and M. M. Labes

Department of Chemistry, Temple University, Philadelphia, Pennsylvania 19122

Abstract

Polarization due to an inhomogeneous space-charge distribution can result in a small pyroelectric coefficient ($\sim$ 1-10 pC $cm^{-2}K^{-1}$) of opposite sign to the large pyroelectric coefficient ($\sim$ 1-4 nC $cm^{-2}K^{-1}$) observed in crystalline poly(vinylidene fluoride) which is largely due to temperature dependent dipole orientation. The former effect is reported in an amorphous copolymer of acrylonitrile (20%) and vinylidene chloride (80%).

It has been theoretically predicted[1] that trapped charge in an insulating film coupled with non-linear thermal expansion of the film can lead to a reversible pyroelectric current. The pyroelectric coefficient in such circumstance is expected to be of the order of a few pC $cm^{-2}K^{-1}$, whereas the observed pyroelectric coefficient of poly(vinylidene fluoride), PVF_2, is three orders of magnitude larger and is predominantly due to dipole reorientation.[2-7] In an effort to examine pyroelectric activity exclusively associated with an inhomogeneous distribution of trapped charge, we turned our attention to those polymers which store charge effectively, but are essentially apolar. An indicator of the ability of a polymer to trap charge is its triboelectric activity. In a recent study of a large group of polymers, Williams[8] noted that PVF_2 and a copolymer of acrylonitrile and vinylidene chloride, P(AN-VCl_2), showed very large triboelectric effects. Thus, P(AN-VCl_2) is an appropriate system in which to observe pyroelectricity, exclusively due to space-charge effects.

The sign of the pyroelectric current in a polymeric film is given relative to the direction of poling, since it is the poling which establishes the essential anisotropy in the film. In a crystalline material, on the other hand, the sign may be established relative to the absolute atomic arrangement. The large reversible pyroelectric current in PVF_2 is such that when the temperature is increased, the electrode which was positive during poling is positive. We shall refer to this as a case of a positive pyroelectric coefficient. The magnitude of the pyroelectric current ϕ is taken as $\phi = \frac{I}{A(dT/dt)}$ where A is the electrode area and dT/dt is the heating rate.

In the sense described, a given model for both poling and subsequent pyroelectric activity is normally expected to be consistent with a given sign. For instance, if the poling process results in an orientation of dipoles in the general direction of the electric field, and if a temperature increase with no field applied results in oscillations of these dipoles above their mean positions, then the sign of the pyroelectric current is unambiguously positive (i.e., the same as is observed in poled PVF_2).

A copolymer of acrylonitrile (20%) and vinylidene chloride (80%) was supplied by Dow Chemical Company (Saran Resin F-310, Lot MMI2II6C4). Films were cast from the solution of the copolymer (5-20% in acetone) in a manner previously described[7] except that annealing was not necessary in these experiments. Usually the thickness of the cast films was in the range of 10 to 20 μ. Electroding, poling and measurements were performed in the manner previously described.[9] Poling of the samples was performed at room temperature and a heating rate of $10^{\circ}C\ min^{-1}$ was employed. For measurements below room temperature, the microscope hot stage (Mettler FP2) which was used to control the sample temperature was placed in a cold chamber cooled with dry ice.

The pyroelectric coefficient in P(AN-VCl_2) (20-80%) is plotted as a function of temperature in Fig. 1 and Fig. 2 for two different samples (A and B). In sample A, a positive pyroelectric current was observed in the first heating cycle. However, in the second and subsequent heating cycles, the polarity of the pyroelectric current was reversed. When the pyroelectricity was measured one day after the third heating cycle, a sharp peak was observed at $34^{\circ}C$. The pyroelectricity in sample B (Fig. 2) shows a similar temperature dependence to that in sample A. In both samples,

the magnitude of the pyroelectricity showed the largest value at $\sim 35^{\circ}C$ and no pyroelectricity was observed above $40^{\circ}C$. The polarity of the pyroelectric current was reversed in the cooling cycles.

The pyroelectric current observed in the first heating cycle (sample A) may be associated with either oriented dipoles or space-charge. Although the material is amorphous[10] and most of the aligned dipoles relax back to the state of random orientation, a small fraction of the alignment could be retained below the glass transition temperature of the material. In the first heating cycle, this residual polarization could contribute to the positive current and subsequently disappear during the first heating cycle.

The negative pyroelectric currents observed in the second and subsequent heating cycles are clearly due to the polarization produced by injected frozen-in space-charge. Such injected charges are trapped in the vicinity of the electrodes and form a fairly stable space-charge even in the amorphous phase. In this case the injected charges have the same polarity as the adjacent electrodes (homocharge), and the polarization produced by such space-charge has a polarity opposite to that of the orientational polarization. It is interesting to note that the pyroelectric coefficient observed is of the same order of magnitude as that predicted by theory[1] assuming the same values for the parameters as in the PVF_2 case. Disappearance of the pyroelectric effect above $40^{\circ}C$ is believed to be related to the glass transition which occurs at about $35^{\circ}C$.[10]

Acknowledgment: This work was supported by the U. S. Army Research Office under Grant No. DAAG29-76-G-0040.

References

1. R. E. Salomon, H. Lee, C. S. Bak and M. M. Labes, J. Appl. Phys. 47, 4206 (1976).
2. M. G. Broadhurst, C. G. Malmberg, F. I. Mopsik and W. P. Harris, "Electrets: Charge Storage and Transport in Dielectrics", p 492, Ed. by M. M. Perlman, The Electrochem. Soc., Princeton, N. J., 1973.
3. H. Ohigashi, J. Appl. Phys. 47, 949 (1976).
4. Y. Wada and R. Hayakawa, Jap. J. Appl. Phys. 15, 2041 (1976).
5. K. Nakamura and Y. Wada, J. Polym. Sci. A-2, 9, 161 (1971).
6. M. Tamura, S. Hagiwara, S. Matsumoto and N. Ono, J. Appl. Phys. 48, 513 (1977).
7. H. Lee, R. E. Salomon and M. M. Labes, Macromolecules 11, 171 (1978).
8. M. W. Williams, J. Macromol. Sci.-Rev. Macromol. Chem. C14, 251 (1976).
9. A. I. Baise, H. Lee, B. K. Oh, R. E. Salomon and M. M. Labes, Appl. Phys. Lett. 26, 428 (1975).
10. R. A. Wessling, "Polyvinylidene Chloride", Gordon and Breach Science Pub., Inc., New York, 1977.

Figure Captions

Figure 1: Pyroelectricity in P(AN-VCl_2) (20-80%) (sample A):

● : first heating cycle;

○ : second heating cycle;

△ : third heating cycle;

□ : fourth heating cycle.

The first to third heating cycles were measured on the same day and the fourth heating cycle was measured on the next day.

Figure 2: Pyroelectricity in P(AN-VCl_2) (20-80%) (sample B):

△ : second heating cycle;

□ : third heating cycle;

○ : fourth heating cycle.

Measurement of pyroelectric current was not possible in the first heating cycle due to high background current. The second to fourth heating cycles were measured one day after the first heating cycle.

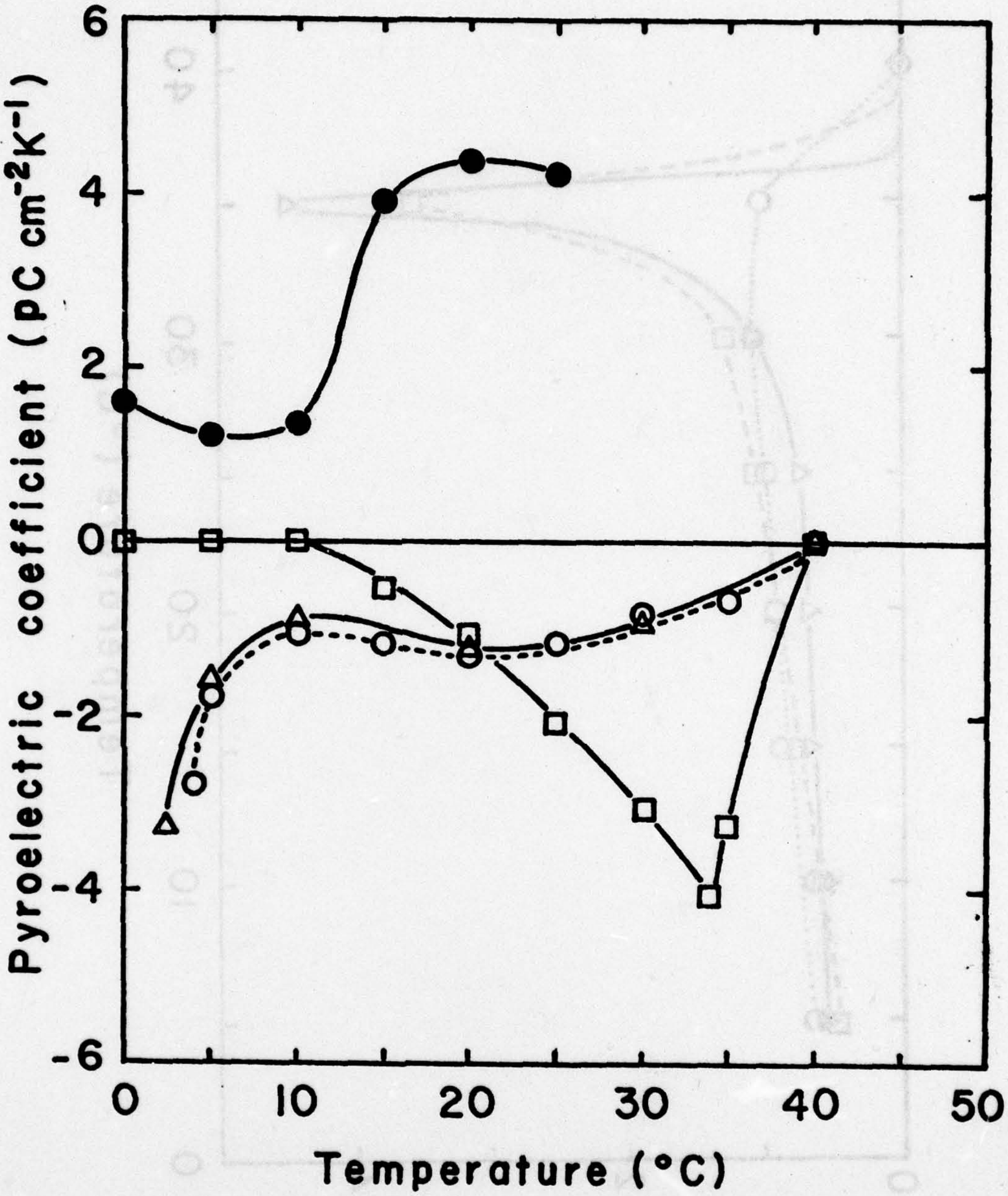

Fig. 1, Lee, Salomon, Lando

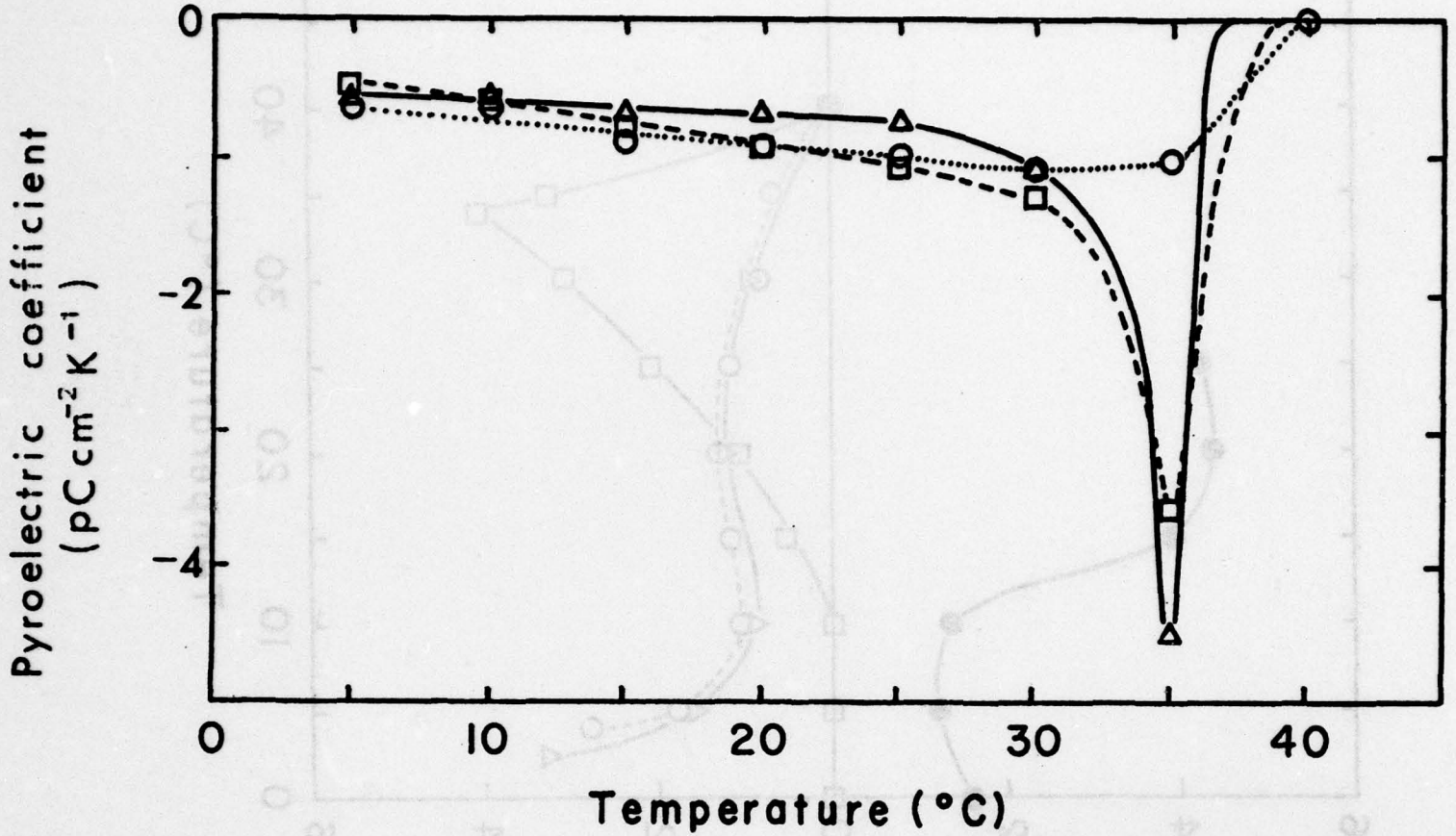
Pyroelectric coefficient
(pC cm⁻² K⁻¹)
0
-2
-4
0
10
20
30
40
Temperature (°C)